Bio-Magnetics Interfacing Concepts: A Microfluidic System using Magnetic Nanoparticles for Quantitative Detection of Biological Species
DARPA Grant No. MDA972-03-C-0100

FINAL TECHNICAL REPORT

September 30, 2004

Submitted to:

Defense Advanced Research Projects Agency
3701 North Fairfax Drive
Arlington, VA 22203-1714

by

Charles J. O'Connor
Advanced Materials Research Institute, College of Sciences
University of New Orleans, New Orleans, LA 70148
Phone: (504) 280-6840, Fax: (504) 280-3185
e-mail address: coconnor@uno.edu
Co-PIs: Josef Hormes (LSU-CAMD)
Nicolas Bazan (LSU-NCE)

This Material is based upon work supported by the
Defense Advanced Research Projects Agency
Defense Sciences Office (DSO)
Effort/Program Title
ARPA Order No. Q472/00/01
Issued by DARPA/CMO under Contract No. MDA972-03-C-0100

Bio-Magnetics Interfacing Concepts: A Microfluidic System using Magnetic Nanoparticles for Quantitative Detection of Biological Species

Charles J. O'Connor
Advanced Materials Research Institute, College of Sciences
University of New Orleans, New Orleans, LA 70148
Phone: (504) 280-6840, Fax: (504) 280-3185
e-mail address: coconnor@uno.edu
Co-PI's: Josef Hormes (LSU-CAMD)
Nicolas Bazan (LSU-NCE)

1. Introduction

Nanoparticles have been used in the form of adjuvants and drug delivery systems [1] and an extensive review of nanoparticles in medicine and pharmacy has been reported [2]. Nanoparticles are of great interest because they exhibit interesting chemical, thermal, optical, electrical and/or magnetic properties, and they find a variety of potential applications in diverse fields of research. Nanoparticles have found considerable utility as controlled drug delivery systems [3]. When suitably encapsulated, a drug or specific specie of interest can be directed to the appropriate site. Because of their small size nanoparticles can easily be injected into the circulatory system.

Magnetic nanoparticles have been used in biomedical research on cell separation, for magnetically targeted drug delivery, for protein and DNA purification, and for contrast enhancement in magnetic resonance imaging (MRI) [3-6]. Recently researchers have investigated the use of magnetic nanoparticles for medical treatment and diagnosis [7-9]. However, currently used magnetic nanoparticles are unstable under normal storage conditions due to aggregation and oxidation. Advances need to be made in order to form more stable formulations. Commercially available magnetic nanoparticles are suitable for cell separation where a large number of particles are used to separate a single cell from a sample. The magnetic moment of these particles is not high enough to enable the separation of single antigen molecules using a single particle. Bio-compatible, high sensitive magnetic sensors capable of detecting single magnetic nanoparticles are needed.

During the last year AMRI and CAMD researchers focused on the development of novel, bio-compatible ferrofluids of functionalized magnetic nanoparticles which are suitable for bioconjugation of antibodies or other active biomolecules. Researchers at AMRI also developed unique nanocomposite particles that are both magnetic and luminescent. Taking advantage of the biochemical expertise of a biochemist at Xavier University (currently at UNO) AMRI researchers reported the successful separation of methastatic breast cancer cells from whole blood [10]. The magnetic properties of particles synthesized by AMRI researchers were characterized by researchers at Magnesensors. Magnesensors has unique SQUID measurement capabilities that enabled high sensitivity measurements of the magnetic properties of magnetic nanoparticles at room temperature. These measurement capabilities were used by Magnesensors in the development of highly sensitive bioassays.

Researchers in CAMD characterized the electronic and geometric structure of magnetic functionalized nanoparticles using EXAFS and XANES techniques. Following a thorough characterization, they made progress towards the development of a "microfluidic tool box" as a flexible, generic platform for fabricating various sensor systems, and develop and fabricate

hybrid (Phase I) and integrated miniaturized (Phase II) sensor systems to detect Bio-warfare species.

The LSU Neuroscience Center of Excellence (LSUNCE) in New Orleans researchers made significant progress towards the development of molecular-recognition processes and the identification of bioreceptor-recognition elements needed to develop nanobiotechnologic approaches to (a) decrease the short-term consequences of mild traumatic head injury (Dr Nicolas Bazan); (b) prevent or slow down laser-induced retinal injury (Dr William Gordon); and c) to effectively manage pain in military personnel (Dr Jian-Guo Cui).

A detailed description of the biomagnetic projects that were conducted by researchers in AMRI, CAMD and LSUHSC are described in the following sections. Collaborative activities between the consortium researchers are noted and emphasized throughout the text in bold font.

PART 1 – AMRI Report

Main Project 1 – Advancing the synthesis of functionalized magnetic nanoparticles

Research activities in the research group of PI O'Connor focused on the synthesis of gold coated magnetic nanoparticles and iron oxide magnetic nanoparticles of higher quality than the current state-of-the-art. The group made significant advances toward the synthesis of stable magnetic nanoparticles that are characterized with small size, narrow size distribution and mono dispersity in aqueous media.

Task 1: Synthesis of gold-coated magnetic nanoparticles

Gold-coated Permalloy ($Fe_{20}Ni_{80}$@Au) nanoparticles have been successfully prepared by a microemulsion process and the results of this study have been published.[1] The particles were prepared by reduction of Fe^{2+} and Ni^{2+} with sodium borohydride in reverse micelles, also known as reverse microemulsions, in which the micelle structure acts as a template, restraining the size of the particles precipitated within the micelles. Au^{3+} was reduced around the Permalloy cores in a second step. The product consisted of 10-15 nm Permalloy nanoparticles encapsulated in 2-4 nm thick Au shells (Figure 1).

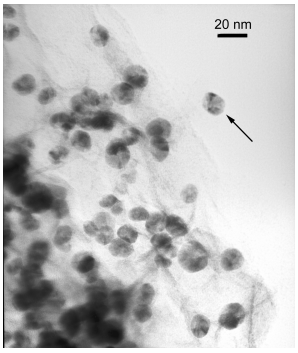

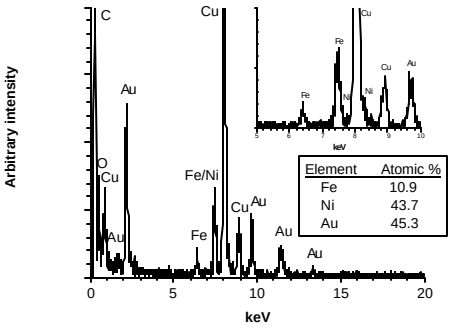

Figure 1 - TEM image of $Fe_{20}Ni_{80}$@Au nanoparticles (left). The EDAX spectrum and elemental composition of the particle denoted with an arrow is presented in the right figure.

SQUID and X-ray diffraction studies of the as-prepared and annealed samples confirmed the composition and superparamagnetic character of the samples:

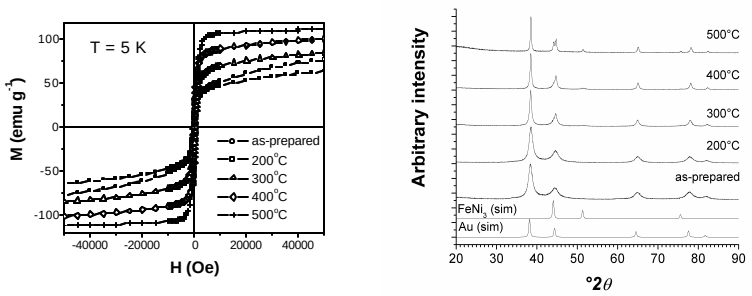

Figure 2 - Magnetization vs. field (left) and X-ray diffraction patterns (right) for $Fe_{20}Ni_{80}$@Au particles annealed at various temperatures.

Gold-coated iron nanoparticles have also been prepared by a non-aqueous method involving the reduction of solvated Fe^{2+} with sodium naphthalide (Na*) reducing agents:

$$Fe^{2+} + 2\ Na^* \rightarrow Fe + 2\ Na^+$$

The Fe metal then serves as a reducing agent for Au^{3+}, which essentially plates to the surfaces of the Fe nanoparticles as some Fe^{2+} is ejected back into solution:

$$5\ Fe + 2\ Au^{3+} \rightarrow 2\ Fe@Au + 3\ Fe^{2+}$$

This method appears to give more uniform shell thicknesses than the microemulsion method, although the particles tend to agglomerate (Figure 3).

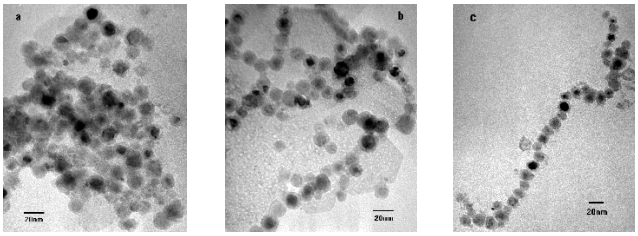

Figure 3 - TEM images of Fe@Au prepared by reduction in non-aqueous solvents.

Problems Encountered

The gold-coated nanoparticles prepared by the above techniques do not exhibit solubility in polar solvents such as water. To address this problem, we attempted to attach mercaptosuccinic acid ($HOOCCH_2(SH)CH_2COOH$) as a capping ligand to the Au shells, believing that the thiol group of MSA would bind to the Au shells while the carboxylic acid groups would allow water solubility.

Two problems were encountered in the process of the MSA derivitazation. First, MSA is not stable in the presence of strong reducing agents like sodium borohydride. Second, the ability of MSA to form Au-S bonds is highly pH dependent. As such, we have been unable to determine the exact conditions necessary for MSA functionalization.

Task 2: Size control of Fe_3O_4 nanoparticles prepared from molecular precursors

We have previously reported a novel synthetic method for ferrite nanoparticles involving the hydrolysis and condensation of molecular precursors.[2] The method produces monodispersed ferrite particles of composition MFe_2O_4 (M = Fe^{2+}, Mn^{2+}, Co^{2+}, Ni^{2+}, Zn^{2+}) but in a limited size range. As part of the DARPA project, we have developed a variant of this technique in which variation of the solvent composition (consisting of a mixture of Diethylene glycol (DEG) and *N*-methyldiethanolamine (DEA)) allows controlled synthesis of Fe_3O_4 from 6 – 18 nm (Figure 5) with very narrow particle size distribution (Figure 6).

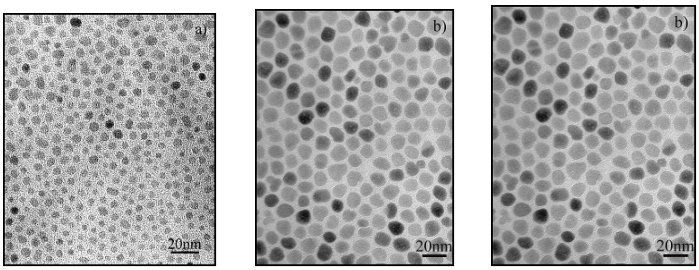

Figure 5 - TEM images of Fe_3O_4 prepared in three different solvent compositions: 100% DEG (left), 50:50 DEG:DEA (center) and 100% DEA (right).

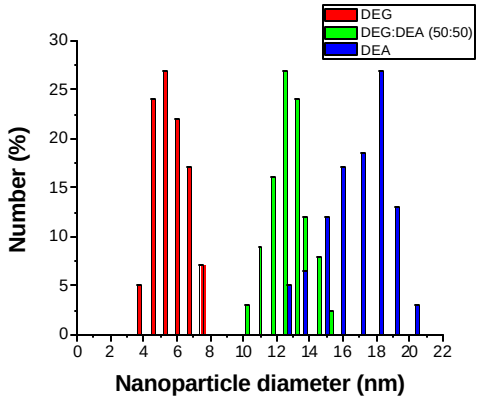

Figure 6 - Size distributions of Fe_3O_4 nanoparticles prepared in three different solvent compositions (see inset legend).

We have also demonstrated that the capping ligands of these particles can be exchanged. Consequently, the surfaces of the particles can be modified to allow solubility in either polar or non-polar solvents. Exchanging oleic acid with betaine, for instances, changes the solubility of the particles from long-chain hydrocarbons to water (Figure 7).

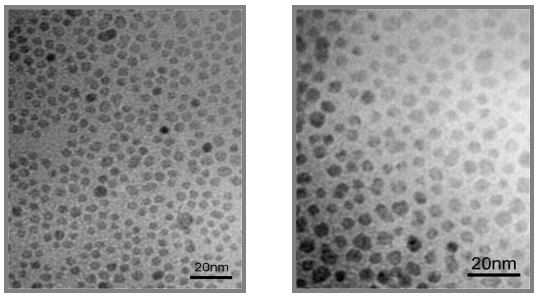

Figure 7 - TEM images of Fe_3O_4 nanoparticles stabilized with oleic acid and dispersed in a hydrocarbon (left) and betaine hydrochloride dispersed in water (right).

Problems Encountered

One of the original goals of the project was to prepare magnetic ferrites as large as 40 nm in diameter for biomedical applications. As yet, we have not been able to find a solvent or combination of solvents that allows synthesis of particles over 18 nm.

Main Project 2 – Synthesis of Magnetic and Magnetic/Luminescent Nanoparticles and their Application in Bioassays and Cell Separation

Task 1- Synthesis and Characterization of Luminescent/ Magnetic Nanocomposite Particles

This objective of this study was to synthesize new nanocomposite nanoparticles that consist of a polymer coated ?-Fe_2O_3 superparamagnetic core and CdSe/ZnS quantum dots (QDs) shell. A single layer of QDs was bound to the surface of thiol-modified magnetic beads through the formation of thiol-metal bonds. Transmission electron microscopy (TEM) and Energy Disperse Spectroscopy (EDS) were used to characterize the size, size distribution and composition of the particles (figure 1 and 2). The average diameter of the nanocomposite particles was determined to be 30 nm with a size variation of ±15%.

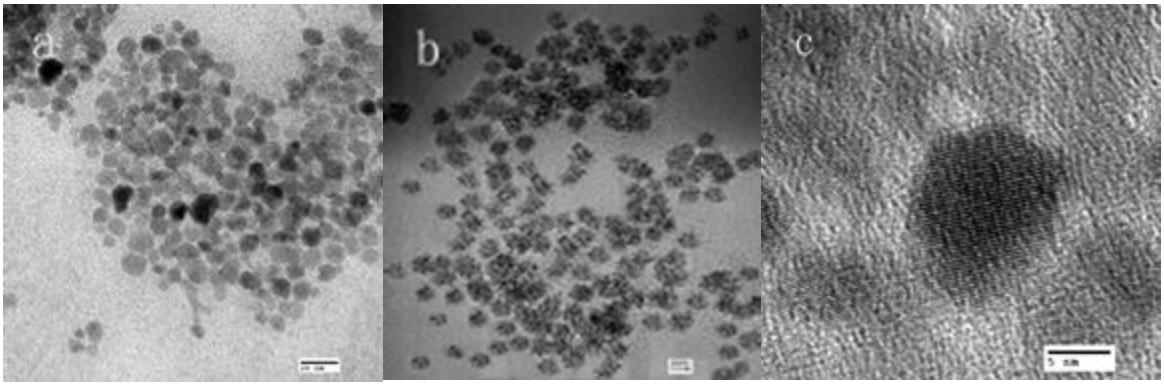

Figure 1 – a) A TEM image of magnetic beads (?-Fe2O3) with polymer coating, the scale bar is 20 nm; b) A TEM image of QDs magnetic beads core-shell nanoparticles. The scale bar is 20 nm. c) A High resolution TEM image of a single magnetic bead coated with quantum dots. The scale bar is 5 nm.

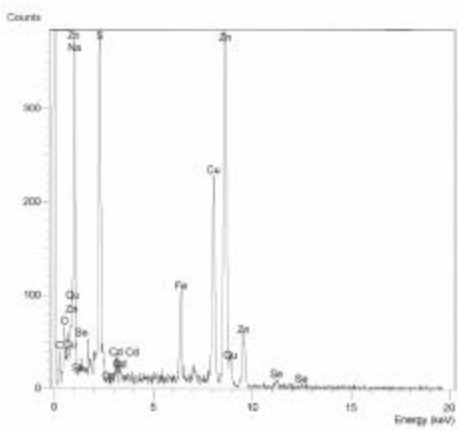

Figure 2 – EDS (Energy Disperse Spectroscopy) spectrum of magnetic beads–QDs core-shell particles showing the presence of Fe, Cd, Zn, S and Se that comprise the nanocomposite particles

The luminescent/magnetic composite nanoparticles were miscible in aqueous solution. A 3-fold decrease in the luminescence quantum yield of the nanocomposite particles and a slight blue shift in their emission peaks compared to individual luminescent QDs were observed. However, the nanocomposite particles were bright and could be easily observed under a conventional fluorescence microscope (figure 3). Additionally, no apparent broadening of the luminescence peak of the QDs could be seen.

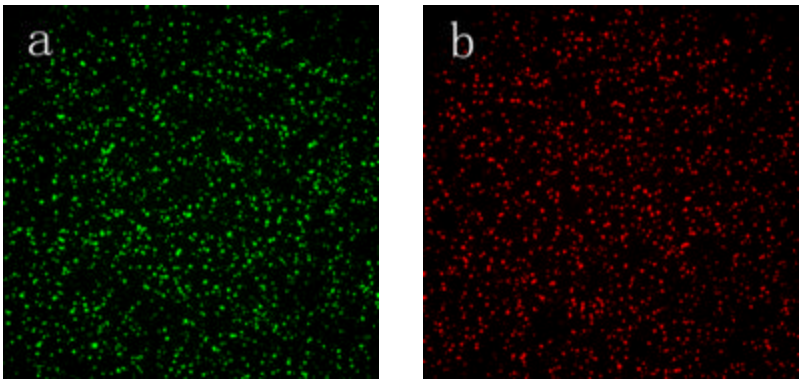

Figure 3 – Digital Fluorescence microscope images of magnetic beads coated with a) 3 nm and b) 5 nm CdSe/ZnS QDs

The composite nanopartic magnet. The new particles could be used in a variety of bioanalytical assays involving luminescence detection and magnetic separation. To demonstrate their utility we immobilized anti cycline E antibodies on their surface and use the antibody coated particles to separate MCF-7 breast cancer cells from serum solutions (figure 4 and 5). Anti cycline E antibodies bind specifically to cycline, a protein which is specifically expressed on the surface of breast cancer cells. The separated breast cells were easily observed by fluorescence imaging microscopy due to the strong luminescence of the luminescent/magnetic nanocomposite particles.

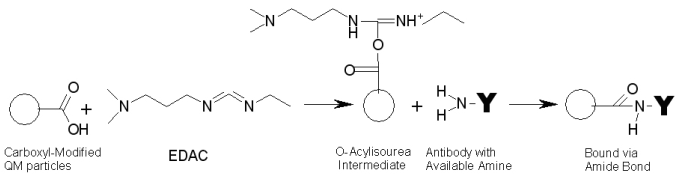

Figure 4 – Schematic of covalent attachment of anti cycline E to the luminescent/magnetic particles using EDAC coupling chemistry

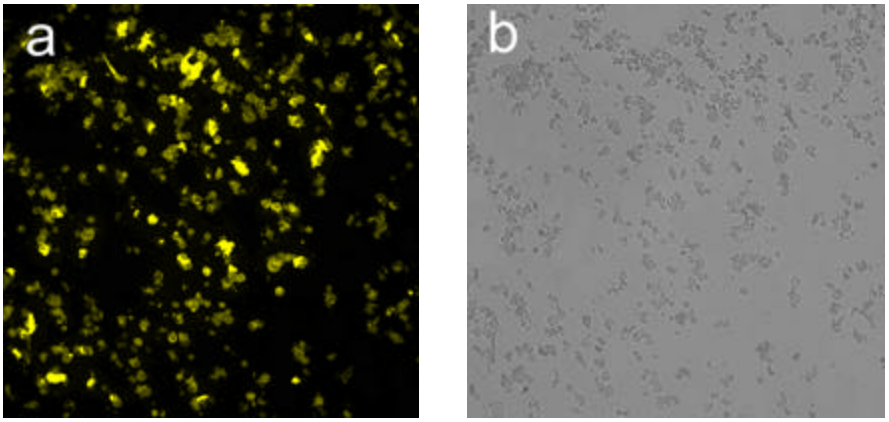

Figure 5 – 10 X Fluorescence (a) and transmission microscopy images of anti cycline E labeled luminescent/ magnetic nanoparticles bound to breast cancer cells.

Problem Encountered

A water-soluble nanocomposite particles consisting of a magnetic core (?-Fe_2O_3) and luminescent quantum dots shell (CdSe/ZnS QDs) were synthesized in an organic/water two-phase mixture. Antibodies for specific breast cancer markers were successfully conjugated to these new nanocomposite particles and were used effectively to separate breast cancer cells from aqueous suspensions and serum. Consistency in the preparation of these nanocomposite particles remain a problem as well as scaling up the synthesis to produce large amount of materials. Future studies will focus on simplifying the procedures to prepare the particles and on forming new formulations of increased stability and utility.

Task 2 - Glucose Oxidase-Magnetite Nanoparticles Bioconjugate for Glucose Sensing

Immobilization of bioactive molecules to the surface of magnetic nanoparticles is of great interest as the magnetic properties of these bioconjugates promise to greatly improve the delivery and recovery of biomolecules in biomedical applications. The objective of this study was to synthesize functionalized magnetite (Fe_3O_4) nanoparticles of 20 nm in diameter (figure 6) and to covalently conjugate the enzyme glucose oxidase to the amino-modified nanoparticles surface (scheme 1).

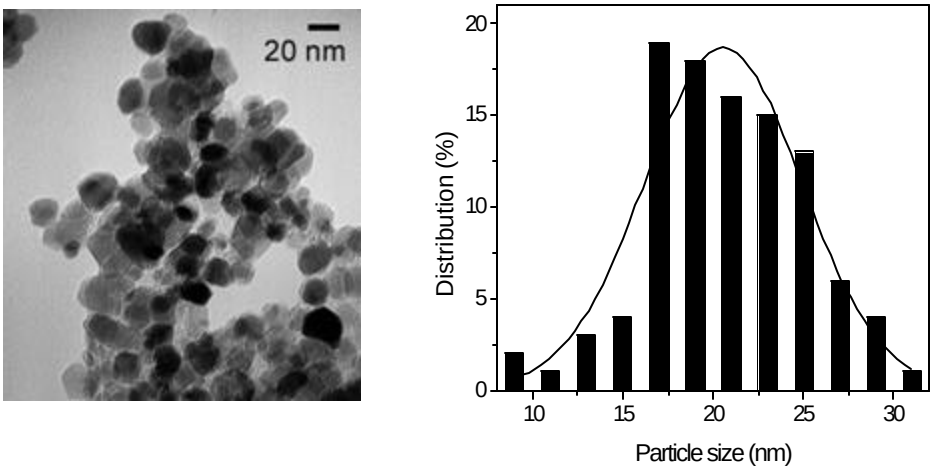

Figure 6 - (a)Transmission electron microscopy (TEM) image of Fe_3O_4 nanoparticles. (b) A histogram describing the particle size distribution as measured from 100 randomly selected particles.

Scheme 1. Preparation of amino-modified magnetic nanoparticles.

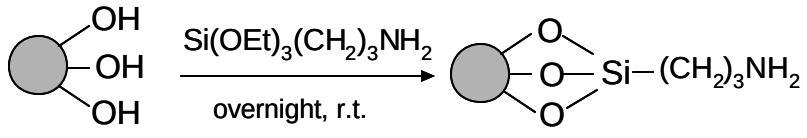

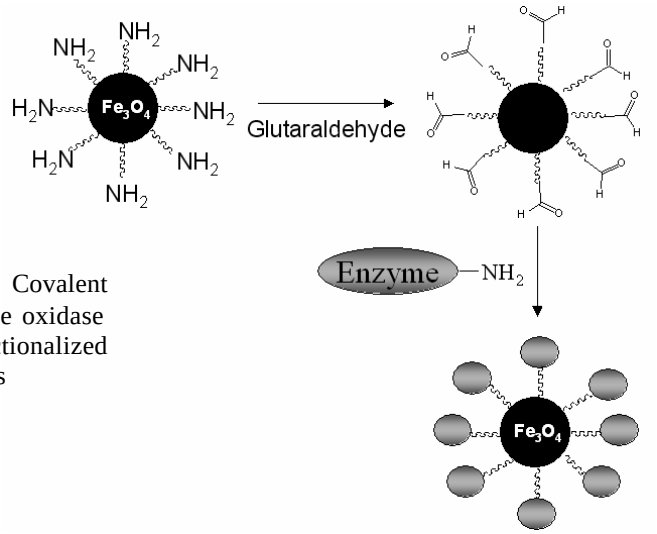

Scheme 2 - Covalent conjugation of glucose oxidase to amino-functionalized magnetic nanoparticles

Functionalization of the magnetic nanoparticles surface with amino groups greatly increased the amount and activity of the immobilized enzyme compared to immobilization procedures involving physical adsorption. The enzymatic activity of the bioconjugate was investigated by monitoring the oxygen consumption during the enzymatic oxidation of glucose using a ruthenium phenanthroline fluorescent complex for oxygen sensing. The glucose oxidase-magnetite nanoparticles bioconjugate could function as nanometric glucose sensors in glucose solutions of concentrations up to 20 mM. Immobilization of glucose oxidase to the nanoparticles also increased the enzyme stability (figure 7). When stored at 4ºC the magnetic bioconjugate suspensions maintained their bioactivity for up to 3 months.

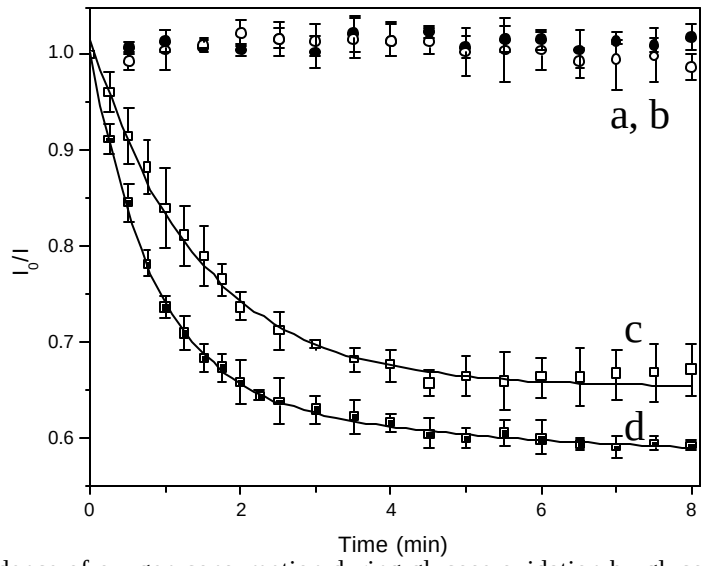

Figure 4. Temporal dependence of oxygen consumption during glucose oxidation by glucose oxidase: Monitoring I_0/I of $Ru(phen)_3$ solutions, where I_0 is the initial fluorescence intensity and I is the fluorescence intensity at a given time interval during the enzymatic reaction. (¦) Free enzyme, (?) glucose oxidase-magnetite nanoparticles bioconjugate – covalent coupling, (?)glucose oxidase-magnetite nanoparticles bioconjugate prepared by physical adsorption and (?) blank experiment without enzyme. Conditions: $[Ru(phen)_3] = 2\times10^{-4}$ M, [glucose]= 100 mM, in phosphate buffer solutions at pH 6.5.

It can be clearly seen that these nanoparticles-bioconjugates showed significant bioactivity with I_0/I reaching steady state (1/e) in about 2 minutes. This was only slightly longer than the oxidation rate shown in curve d (¦) for a solution of free glucose oxidase containing similar amount of glucose oxidase as determined by UV absorption measurement at 280 nm. It is fair to conclude that functionalization of the magnetic nanoparticles surface with amino groups greatly increased the amount and activity of immobilized enzyme molecules compared to the amount and activity of enzyme molecules in bioconjugates that were prepared by physical adsorption.

Problems Encountered

The study revealed that the glucose oxidase - magnetite nanoparticles bioconjugate could be separated magnetically from the analyte sample. Therefore, it was possible in principle to reuse the glucose oxidase- magnetic nanoparticles bioconjugate for successive glucose measurements in multiple samples. However, our results showed a significant degradation in enzymatic activity following two successive runs of glucose measurement. This was attributed to loss of particles during the magnetic separation-redispersion cycles and aggregation of the particles following the magnetic separation. We are currently exploring ways to encapsulate magnetic nanoparticles in larger nanometric silica particles to minimize particle losses and effects of aggregation on the enzymatic activity of the bioconjugates. We are also exploring ways to covalently attach oxygen sensitive fluorescence dyes to the surface of the nanoparticles aiming to develop magnetic/luminescent nanoparticles-based glucose sensors.

Pilot Project 1 – Weilie Zhou

Task Objective

The objective of this project is to immobilize magnetic nanoparticles to silica hollow structures for drug delivery applications

Technical Problems Encountered and General Methodologies

One gram of spherical calcium carbonate nanoparticles synthesized by a high gravity technique with a diameter of 25-60 nm, was dispersed in a mixture of ethanol and distilled water by sonication. Then 4mL of magnetic fluid (Fe_3O_4 nanoparticles dispersed in methanol, ~14mg/mL) and 1.04 g of TEOS and 50 mL of ammonium hydroxide were added into the suspension to reach a pH of ~11. The suspension was stirred by a mixer for 2 hrs, aged for 4 hrs at room temperature, and subsequently filtered and rinsed with distilled water and ethanol. The filter cake was dried at 60ºC for ~6 hrs and then immersed in an acetic acid solution ($HAc:H_2O$=1:10, pH=2.5) for ~12 hrs. The product was afterwards filtered, rinsed with distilled water, and dried at 60ºC for ~7 hrs to yield MHSNS.

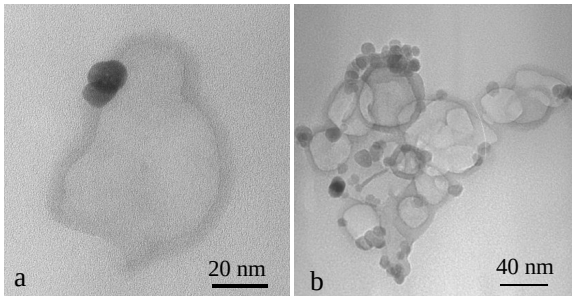

Figure 1 – (a) Single and (b) aggregated magnetic nanoparticles containing silica hollow structures

Transmission electron micrographs of magnetic nanoparticles-containing silica hollow structures are shown in figure 1. The silica hollow nanospheres have a diameter of 25-60 nm with a shell thickness of about 10 nm. Fe_3O_4 nanoparticles with a diameter of 10 nm are mostly embedded in the silica shells, which gives hollow silica nanospheres magnetic properties. TEM observations show a few magnetic particles, sticking on the surface of hollow silica nanoshperes, which has less influence on the properties. It is noted that no residual $CaCO_3$ nanoparticles were detected by EDS analysis, which implied the weak acetic acid penetrated the shell of silica effectively etched away the $CaCO_3$ nanoparticle cores, and generated the hollow structures.

Figure 2 – Zero field cooled (ZFC) and field cooled (FC) Magnetic measurements of the magnetic nanoparticles-containing silica hollow structures

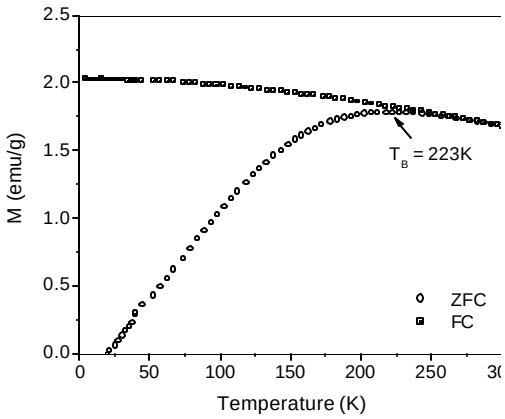

Zero-field-cooled (ZFC) and field-cooled (FC) magnetization data in the temperature range of 5 to 300 K are shown in figure 2. In the ZFC experiment the initial field was set to zero as the sample was cooled to the lowest temperature. A field of 100 Oe was then applied and the magnetization was measured as the sample was heated from 5 to 300 K. In FC experiment a field of 100 Oe was applied as the sample was cooled to the lowest temperature and the magnetization was measured as the sample was heated from 5 to 300 K in the field of 100 Oe. The ZFC curve shows a maximum at 223 K, which is the blocking temperature (T_B). Such a behavior is characteristic of superparamagnetism and is due to the progressive blocking of the magnetic moment of nanoparticles when decreasing the temperature.

Figure 3 – Field dependent hysteresis loop of the magnetic nanoparticles-containing silica hollow structures

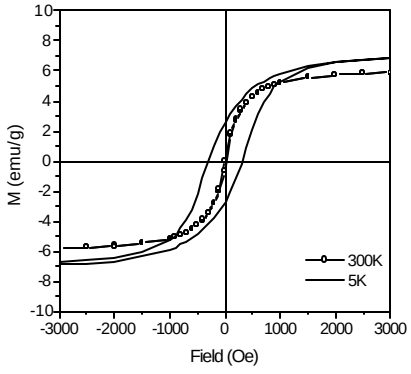

Figure 3 shows the field dependent hysteresis loops of the magnetic nanoparticles- containing silica hollw structures. The particles exhibit superparamagnetism and ferromagnetism above and below the blocking temperature, respectively. The magnetization vs. field data at 5 K displays hysteresis with saturation magnetization of 7.8 emu/g (at the field of 50000 Oe) and coercivity of 316 Oe, which confirms that particles were ferromagnetic below the blocking temperature. The absence of coercive hysteresis at 300 K is characteristic of superparamagnetic nanoparticles.

Important Findings and Conclusions

Magnetic hollow silica nanospheres were successfully synthesized using calcium carbonate cores as sacrificial templates and TEOS and magnetite as precursors. The TEM results showed that the silica structures consisted of a thin layer of silica embedded with Fe_3O_4 nanoparticles. No calcium carbonate nano-templates were observed after the acid etching. Even though the magnetite nanocomposites were subjected to weak acetic acid etching and low temperature heating process, the magnetic properties of Fe_3O_4 nanoparticles embedded inside the silica shells still remained. Our previous study indicated that hollow silica synthesized using calcium carbonate as template has a large surface area and is favorable for drug adsorption and delivery. It is therefore expected that MHSNS can be exploited as delivery vehicles and supports in bioscience applications.

Pilot Project 2 – Paul Hanson

Objective - Use a biological system to drive the self-assembly of Au/Ni nanowires and develop a *de novo* bio-inorganic material.

Strategy - Link cysteine containing beta-amyloid peptide fragments to the Au/Ni nanowires, through an Au-S bond, to use the fibril forming properties of the peptides to organize the Au/Ni nanowires.

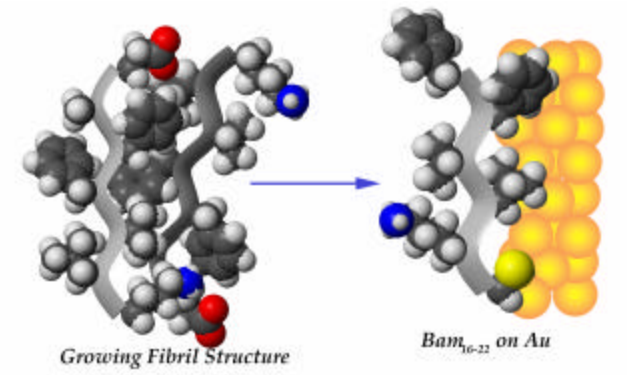

Figure 1 - Van der Waals representation of ßam$_{16-20}$ on a model Au surface. The presence of ßam$_{16-20}$ is projected to act as a seed for initiating amyloid fibril formation (ßam$_{16-22}$) around the Au/Ni super-lattice wire.

Technical problems encountered:

1. Development of a method that permits reproducible control of the Au/Ni super-lattice.
2. Following the adsorption of the polypeptide upon the Au/Ni super-lattice surface.

Technical results

Peptide fragments from $A\beta_{1-40}$ have been synthesized by FMOC synthesized with the purpose of using them to assemble Au/Ni super-lattice nanowires in a one- or two-stage process. The two sequences are

βam_{16-20} CKLVFF

βam_{16-22} KLVFFAE

and they are aligned to reveal their common sequence (KLVFF). In βam_{16-20} , the peptide contains a non-native cysteine that leads to the adsorption of this peptide onto the Au super-lattice segments of a a Au/Ni wire through formation of a Au-S bond. The βam_{16-20} peptide has been shown to have a high affinity for amyloid fibrils. Our hypothesis is that once βam_{16-20} has been attached to the Au/Ni wires, βam_{16-22} can then be added to the mixture to drive the association of the amyloid fibrils around the wire (figure 1).

Adsorption of the βam_{16-20} peptide is followed by a reduction of the peptide area detected by HPLC as a function of time (Figure 2, triangles). In solution alone, βam_{16-20} reveals a bi-exponential decay over 24 hours. Within the first five hours, the concentration of peptide goes through a fifty percent reduction and then remains essentially constant for the remainder of the experiment. The reduction of the peptide's concentration is hypothesized to be the result of the peptide's tendency to aggregate.

Upon mixing βam_{16-20} with wires, from collaboration with Dr. Wiley of the University of New Orleans chemistry department, the peptide is sequestered from solution through covalent attachment of the cysteine's thiol with the exposed Au-surface (figure 1). Unlike the sample without Au/Ni superlattice wires, the area as a function of time remains constant but at a significantly reduced concentration than in the sample without wires. The amount of peptide used between the two experiments is identical within experimental error. The result indicates that 1, the difference in concentration is due to adsorption of the peptide onto the Au segments of the wires. The result also suggests HPLC can be used as a tool determining the load of peptide onto the Au/Ni wires.

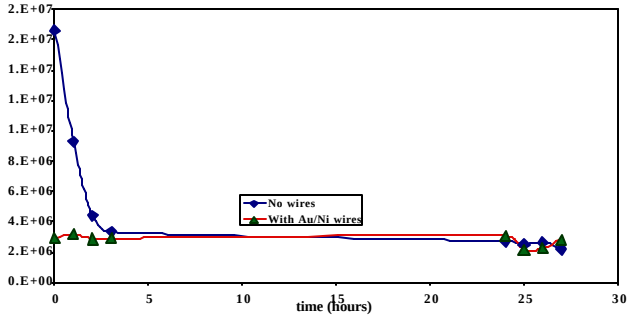

Figure 2 - Without wires present, ?am$_{16-20}$ aggregates with in a bi-exponential process. The peptide is immediately adsorbed in the presence of the Au/Ni superlattice wires.

This interpretation can be tested by increasing the load of βam_{16-20} on the wires to the point that the original bi-exponential curve is recovered. Under these conditions, the conclusion can be reached that the Au/Ni wires have loaded the maximum amount of βam_{16-20}. It is interesting to note from figure 4 the speed of the peptide's loading process. The adsorption is complete within the dead time of loading the first sample on the HPLC (~2 minutes). HPLC provides a route to quantifying the amount of peptide loaded onto the wires as well as the time taken to achieve that load. In combination, these provide a mechanism for exploring the factors that affect protein adsorption on surfaces.

The next step will be to add the amyloid forming peptide βam_{16-22} to the βam_{16-20}•wire complex. The hypothesis is βam_{16-20} will act as a seed to direct amyloid fibril organization around the Au/Ni superlattice wires. As a test of this hypothesis, Au/Ni super-lattice wires treated with βam_{16-20} were examined by scanning and transmission electron microscopy (SEM, TEM respectively). The βam_{16-20} peptide is known to aggregate and as such, examination by SEM and TEM seemed a reasonable first test of the organizational behavior of the peptide. The SEM data, figure 3a, reveals that the Au/Ni wires associate such that all the Au segments are coincident. In figure 3b, TEM data reveals the presence of amorphous material between the wires (translucent portion) that holds the two Au/Ni super-lattice wires together.

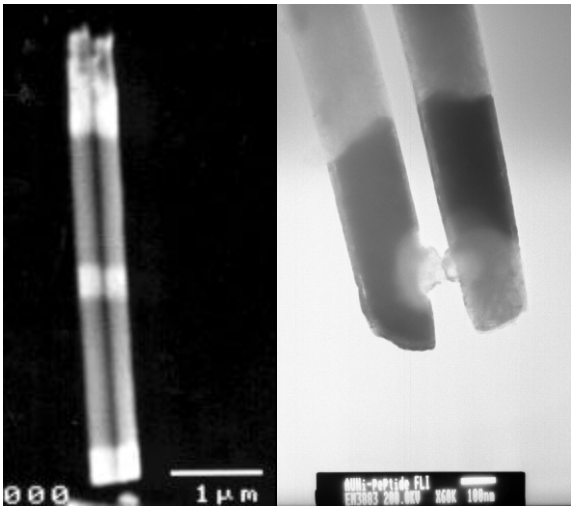

Figure 3. (a) SEM of Au/Ni super-lattice wires with $A\beta_{16-20}$ incorporated on the Au lattice. (b) TEM revealing the $A\beta_{16-20}$ (translucent) that holds the wires together along the Au segments (darker portion).

The results suggest that in the presence of βam_{16-20}, with its built-in aggregation properties, will direct the assembly of these Au/Ni super-lattice wires. Furthermore, the results give credence to the idea that fibril formation around the wires will occur upon addition of βam_{16-22} to the βam_{16-20}•wire composite.

Importance of Findings

A complete understanding of the factors affecting protein adsorption on surfaces must be made before the benefits of nanotechnology are to be fully realized. For example, the folding of proteins on nanoparticle surfaces will play an important role in their behavior as sensors. In a move towards understanding the factors affecting protein adsorption on surfaces, the strategy to

our objective involves using the self-organizing biological system of β-amyloid fibrils to direct the assembly of nano-scale Au/Ni nanowires. The magnetic susceptibility of the Ni component within the wires permits use of an applied magnetic field to provide a further level of organization. The data from this work will be used to provide details about the factors affecting protein-surface interactions and surface coverage. Utilizing the self-assembly of β-amyloid peptides into fibrils to organize Au/Ni super-lattice wires is an example of a bottom→up approach to nanoscale assembly. The outcome of the project is the development of an organizable nanoscale system controlled by a biological template.

Pilot Project 3 – Matt Tarr - Sonochemical Synthesis of Functionalizable Magnetic Nanoparticles

Objectives

1) To optimize the sonochemical formation of gold coated magnetic nanoparticles
2) To develop sonochemical methods for producing magnetic nanoparticles coated with silica
3) To investigate the controlling factors of sonochemical coating of magnetic seed particles so that better control of such systems can be achieved.

In addition to the above listed objectives, a longer term aim is to utilize the gold and/or silica coated nanoparticles produced in this project for ongoing collaborative studies on biomedical and biosensor applications.

Technical Problems Encountered

While gold-magnetite nanocomposite materials have been prepared, they do not have the desired core shell structure in which magnetite forms the core of the particle and is fully coated by a gold shell. This difficulty was anticipated since gold and magnetite are known to have poor cohesion.During the sonochemical process, capping ligands that are present on the surface of preformed magnetite particles are partially or fully removed. This removal results in increased rates of particle agglomeration, which is undesirable. To date, all studies have focused on gold-magnetite materials. Due to the extent of effort directed at this portion of the project, studies on silica-magnetite materials have not yet begun.

General Methodologies

A sonochemical technique was used to prepare gold-magnetite nanocomposites. A titanium horn, high power (600 W) sonicator was used in these studies. Magnetite particles were independently prepared using a microemulsion method. The preformed magnetite particles were suspended in aqueous solutions of $HAuCl_4$ (0.1 mM) and were sonicated under argon with an added hydroxyl radical scavenger. Scavengers utilized included methanol, diethylene glycol, and oleic acid. The resulting nanoparticles were separated magnetically and washed three times with water. After the final wash, the water was removed and the particles were resuspended in ethanol. Transmission electron microscopy (TEM) was used to determine particle size and morphology, including elemental analysis using energy dispersive spectroscopy (EDS). Inductively coupled plasma atomic emission spectroscopy was used for elemental analysis of bulk samples. Magnetic properties of nanomaterials were evaluated using SQUID magnetometry.

Technical Results

Sonication of magnetite nanoparticles in the absence of $HAuCl_4$ did not cause any observable changes in the TEM images of the magnetite particles. In the presence of $HAuCl_4$, sonication resulted in the appearance of a red or purple coloration of the particles, as depicted in Figure 1. Exposing these materials to a magnetic field resulted in removal of all colored material from the liquid. This result indicates that the gold particles must be physically or chemically attached to the magnetite.

Figure 1 - Gold-magnetite nanocomposite materials suspended in ethanol prior to (a) and after (b) magnetic separation. The pink/purple color is from the gold nanoparticles. Note that all color is removed after separation, indicating that the gold was attached to the magnetite.

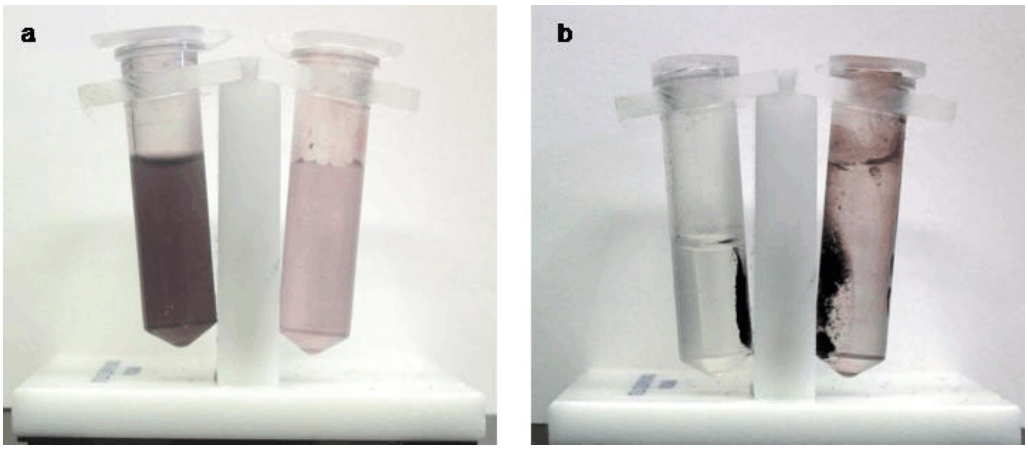

This attachment is at least strong enough to cause the suspended gold particles to migrate with the magnetite in a magnetic field. TEM images of these particles revealed the presence of both gold and magnetite forming a nanocomposite material (see Figure 2).

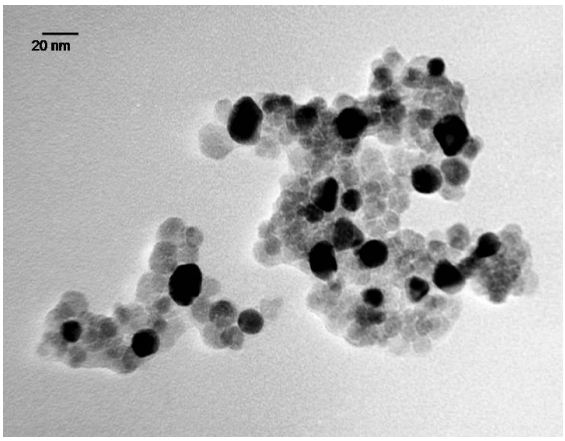

Figure 2 - TEM image of gold-magnetite nanocomposite material formed by sonication of magnetite in aqueous $HAuCl_4$ with added methanol. Dark particles are gold, grey particles are magnetite.

Observation of the particles in Figure 2 suggests a high degree of agglomeration between magnetite particles. This degree of agglomeration is likely due to the removal of the initially present capping ligand during the sonication process.

EDS analysis of the particles indicated the presence of both iron and gold, as illustrated in Figure 3. The data presented in this EDS spectrum were collected from multiple particles, and is therefore representative of the composite material. Additional EDS spectra collected on single particles verified that the dark particles in the TEM image (Figure 2) are in fact gold and the grey particles contain iron as the only metal.

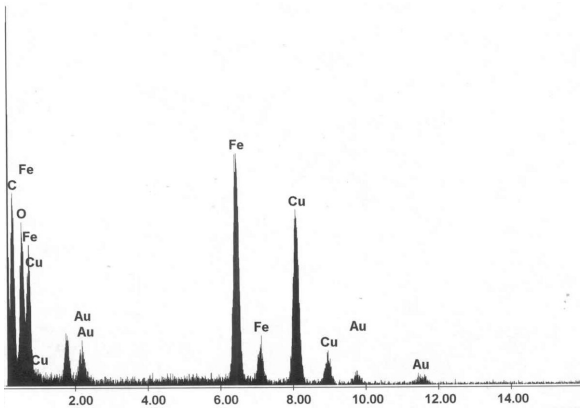

Figure 3. EDS spectrum of composite particles depicted in Figure 1. Copper and carbon signals are from the TEM grid.

The gold-magnetite nanocomposite material was also characterized to determine its magnetic properties using a SQUID magnetometer. Substantial changes in the magnetic properties of these materials were observed compared to the untreated magnetite precursor material. Figure 4 compares the magnetization vs. temperature behavior of the untreated magnetite and the gold-

magnetite nanocomposite material. While the general shape of these curves is similar, the gold-magnetite nanocomposite material exhibited a substantially higher magnetization at 300 K of about 23 emu/g compared to 14 emu/g for the untreated magnetite. In both cases, the magnetization was normalized to total mass of magnetite in the sample. In addition to the differences in magnetization, the coercivity of the sample changed upon formation of the nanocomposite material. The untreated magnetite had an observed coercivity of 75 Oe, while the gold-magnetite nanocomposite material exhibited a substantially increased coercivity of 200 Oe. These data are depicted in Figure 5. Also apparent in this figure, is the significantly larger saturation magnetization (M_s) for the nanocomposite material (M_s ~ 125 emu/g) compared to the untreated magnetite (M_s ~ 90 emu/g).

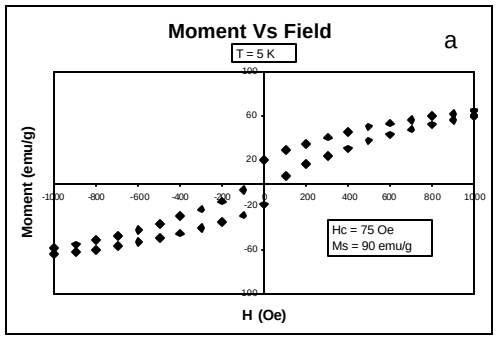

Figure 4 - Magnetization vs. temperature for magnetite nanoparticles (a) and gold-magnetite nanocomposite material (b). In each panel, the top curve is for the field cooled sample and the bottom curve is for the zero field cooled sample.

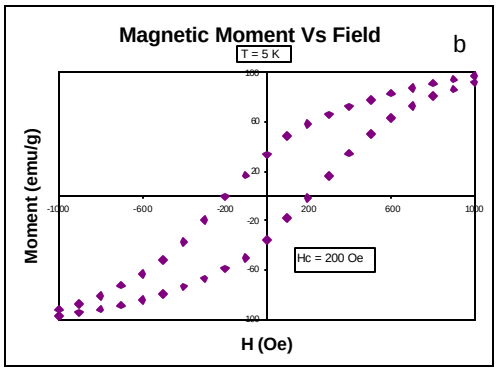

Figure 5 - Hysteresis loops for untreated magnetite (a) and gold-magnetite nanocomposite material (b).

The changes in magnetic properties are most likely due to changes in the surface characteristics of the magnetite. During sonication, the capping ligands initially present can be removed. Removal of these capping ligands could cause a change in the surface charge or magnetic domains. Surface modification of the magnetite is also possible under the reactive conditions that occur during sonication. In addition, interactions between magnetite particles could be enhanced by their direct contact, which is not possible with capping ligands present. Finally, interaction of the magnetite surface with gold could contribute to changes in the surface states, yielding altered magnetic properties. A control experiment was performed in which magnetite was sonicated under identical conditions but with no $HAuCl_4$ present. The magnetic properties for these particles showed decreased saturation magnetization (M_s ~ 5 emu/g) compared to untreated magnetite. The fact that magnetite sonicated in the absence of gold exhibited decreased magnetization and magnetite sonicated in the presence of gold showed increased magnetization, indicates that interaction of gold with magnetite appears is a significant factor in controlling the magnetic properties of the composite material.

Additional investigations utilized diethylene glycol or oleic acid in place of methanol. These additives served two purposes: 1) they acted as hydroxyl radical scavengers, thereby promoting the reducing conditions needed for gold metal formation and 2) they acted as capping ligands for the particles. In addition to these functions, the additives were also found to change the gold particle size and the Fe/Au ratio in the composite materials. Therefore, adjusting the identity and amounts of these additives may provide a mechanism for preparing gold-magnetite nanocomposite materials with a range of selected Fe/Au compositions and particle sizes.

Figure 6 depicts the TEM for gold-magnetite nanocomposite material formed with diethylene glycol as an additive, and Figure 7 presents the TEM image when oleic acid was used. When diethylene glycol was used, more uniform gold particles were observed. In addition, the Fe/Au ratio decreased compared to the material prepared using methanol as an additive. With oleic acid added, substantially smaller gold particles were observed, and the Fe/Au ratio decreased even further. EDS data collected for these particles verified the presence of both gold and iron in the nanocomposite material. As for the samples prepared with methanol, these particles were collected by magnetic separation, indicating that the gold and magnetite were bound together strongly enough to remain attached and migrate together in the magnetic field.

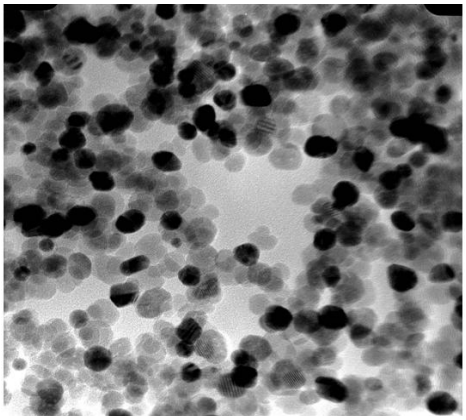

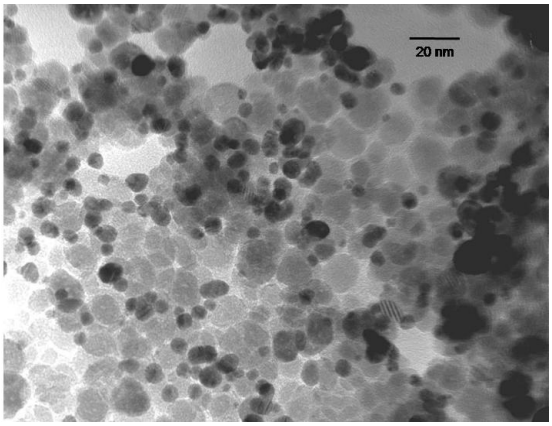

In addition to the studies utilizing gold, we have also investigated the ability to form silver-magnetite nanocomposite materials. Initial experiments met with limited success. While silver-magnetite nanocomposites were formed, there were few silver particles, and those that were formed were relatively large (~50-100 nm).

Importance of Findings

The experiments conducted to date have resulted in a novel method for preparation of gold-magnetite nanocomposite materials. These materials substantially maintain the optical properties of gold. At the same time, the gold can be separated or otherwise manipulated with a magnetic field. No prior reports have indicated success in making such materials. The new methodology also includes parameters that can be adjusted to vary the Au/Fe ratio and particle sizes of the gold structures within the nanocomposites. These new particles have potential use in biomedical applications, in sensor applications, and in electronic, optoelectronic, and magnetooptic devices.

Furthermore, the fundamental interactions occurring at the gold-magnetite interface are poorly understood. These new nanocomposite materials provide an opportunity to study these interfaces and gain knowledge about interparticle interactions within nanoscale materials.

Implications for Further Research

The gold-magnetite nanocomposite materials prepared to date have a number of interesting properties, including altered magnetic properties, altered optical properties, and altered magnetooptical properties. The gold in the nanocomposites is bound strongly enough to the magnetite that the gold particles can be manipulated (i.e. moved) in a magnetic field. Furthermore, the nanocomposite materials have exposed gold surfaces that are available for surface modification. These particles therefore provide the potential for magnetically directed drug delivery, detection of specific antigens, or enhancement of medical imaging techniques. Continuing studies will further investigate how sonochemical preparation parameters affect the particle morphology. The ability to produce a wide range of nanocomposite materials with different size ratios among the metal and magnetite particles seems feasible with some additional tuning of the current methodology. Furthermore, additional noble metals (e.g. silver) can also yield nanocomposite materials with magnetite. However, optimized parameters for other metals have not yet been devised.

Publications

[1] "Synthesis and magnetic properties of Au-coated amorphous $Fe_{20}Ni_{80}$ nanoparticles," B.L. Cushing, V.O. Golub, and C.J. O'Connor, *J. Phys. Chem. Solids*, 2004, *65*, 825-829.

[2] "Reactivity of 3d Transition Metal Cations in Diethylene Glycol Solutions. Synthesis of Transition Metal Ferrites with the Structure of Discrete Nanoparticles Complexed with Long-Chain Carboxylate Anions," D. Caruntu, Y. Remond, N.H. Chou, M.J. Jun, G. Caruntu, J. He, G. Goloverda, C. O'Connor, and V. Kolesnichenko, *Inorg. Chem.*, 2002, *41*, 6137-6146.

[3] "CdSe/ZnS Quantum Dots-Magnetic Beads Core-Shell Nanocomposite Particles for Cell Separation," Desheng Wang, Jibao He, Nitsa Rosenzweig and Zeev Rosenzweig, *Nano Letters*, 2004**,** 4(3); 409-413.

[4] "Glucose Oxidase-Magnetite Nanoparticles Bioconjugate for Glucose Sensing," Liane M. Rossi, Ashley D. Quach and Zeev Rosenzweig, *J. Anal. and Bioanal. Chemistry* (published online, in press, 2004).

[5] "Fabrication of Nanoporous Silica Nanospheres and Nanotubes by Inorganic and Organic Double Templates," Jian-Feng Chen, Runjing Liu, Dapeng Cao, Zhigang Shen, Jimmy Yun, Jiexin Wang, Lei Shao and Weilie L. Zhou, *Mat. Res. Soc. Symp. Proc*., 823, W.16 (2004).

[6] "Fabrication of Magnetic Hollow Silica Nanospheres for Bio-Applications," L. Shao, D. Caruntu, J.F. Chen, C.J. O'Connor, and W.L. Zhou, 49th Annual Conference on Magnetism & Magnetic Materials, (2004) (submitted J. Applied Phys.).

Presentations

"Luminescent/Magnetic nanoparticles in Bioassays," Desheng Wang, Nitsa Rosenzweig and Zeev Rosenzweig, Pittcon 2004, New Orleans, LA, March 2004.

"Magnetic Nanoparticles Bioconjugates for glucose sensing," Liane Rossi, Ashley Quach and Zeev Rosenzweig, Gordon Research Conference on Bioanalytical Sensors, Oxford, UK, July 2004.

"Novel Synthetic Routes to Formation of Magnetic Nanocomposites with Noble Metals," M. A. Tarr, A. Pradhan, and T. T. Poché, ACS National Meeting, Philadelphia, PA, August, 2004.

"Biomagnetics: Sonochemical Synthesis of Gold-Magnetite Nanocomposite Particles," Anindya Pradhan, Teyoko Poché, and Matthew Tarr, DARPA AMRI Symposium, February, 2004, New Orleans, LA

"Fabrication of Nanoporous Silica Nanospheres and Nanotubes by Inorganic and Organic Double Templates," Jian-Feng Chen, Runjing Liu, Dapeng Cao,1 Zhigang Shen,Jimmy Yun,Jiexin Wang,1 Lei Shao and Weilie L. Zhou, Mat. Res. Soc. Symposium, 2004.

"Fabrication of Magnetic Hollow Silica Nanospheres for Bio-Applications," L. Shao, D. Caruntua, J.F. Chen, C.J. O'Connor, and W.L. Zhou, 49th Annual Conference on Magnetism & Magnetic Materials, 2004.

PART 2 – LSU-CAMD Report

Bio-Magnetics Interfacing Concepts: A Microfluidic System using Magnetic Nanoparticles for Quantitative Detection of Biological Species

(Subcontractor: LSU/CAMD)
Center for Advanced Microstructures and Devices
Louisiana State University
6980 Jefferson Hwy. Baton Rouge, LA70806

Bio-Magnetics Interfacing Concepts: A Microfluidic System using Magnetic Nanoparticles for Quantitative Detection of Biological Species

(Contractor: LSU/CAMD)
Author / Authors
Center for Advanced Microstructures and Devices
Louisiana State University
6980 Jefferson Hwy. Baton Rouge, LA70806

ABSTRACT

Miniaturized microfluidic/magnetic sensing devices for chemical/bio warfare detecting have attracted tremendous attentions by war-zone personnel and first responders. These kind of sensing devices have potential to be robust, portable, and highly reliable in noisy environments. There are many sensors and assay protocols have been developed for aforementioned applications, but most of them are still in the stage of discrete component with simple functionality/functionalities. This study has focused on a systematic approach for a microfluidic—GMR sensor based diagnosis system for chemical/Bio warfare detection. The work during this period has been concentrated on following aspects: (1) wafer scale integration of microfluidic channels with GMR sensor chip, (2) optimization of excitation and measurement circuitry for high resolution detection, (3) magnetic nanoparticle development, (4) sensor surface functionalization and (4) system integration. Current results show that CAMD, collaborated with NVE, has developed a prototype processing procedures to make a wafer scale integration of microfluidic channels with GMR sensors. First generation micro-macro fluidic connectors, which have potential to be made by LIGA technique, have also been developed. Prototype micro-mixer and micro-valve modules for future system integration have been designed and fabricated. A series of nano magnetic particles with enhanced magnetic momentum have been fabricated through this project. Electronic set up for high resolution GMR measurement has also been finished and show a detection limit of 100 micro beads at this point. The bio surface functionlization is under the way for developing so that it can adapt the complexities caused by integration of microfluidic channels with GMR sensors.

TASK OBJECTIVES

Five major objectives have been addressed during this period of the project, which are: (1) Wafer scale integration of microfluidic channels with NVE GMR sensors, (2) Design and fabrication of micro-macro fluidic connectors, (3) Development of magnetic nanoparticles with improved properties, (4) optimization of GMR circuitry for high sensitivity and high resolution measurements, (5) Sensor and magnetic particles surfaces functionalization for high sensitivity and specificity assays.

1. Wafer Scale Integration of Microfluidic Channels with NVE GMR Sensors

Technical Problems. One of the key issues for GMR sensor based bio/chemical assays is to integrate the microfluidic structures to the sensors since majority of assays are conducted in aqueous environment. Tremendous efforts have been made to make efficient integration of microfluidic structures to the sensors. Conventional procedures for integrating silicon/glass based microfluidic structures to GMR sensors involve silicon/silicon wafer-bonding or silicon/glass anodic bonding using high temperature and high electrical current, which will destroy the GMR sensors [1]. Most common practice in microfluidic/GMR sensor integration is using hybrid approaches by adding-on polymer based fluidic structures (such as PDMS fluidic structures) on the surface of individual GMR sensor. This kind of approach is very hard to control quality, low in yield, high in cost, and very difficult to make commercial available disposable detecting chips[2]. Therefore, developing a wafer scale microfluidic/GMR sensor integration technique compatible with GMR sensor fabrication and packaging processes will be a key issue for making commercially available, disposable, microfluidic based GMR sensing chips.

General Methodology. Starting from February 2004, together with NVE we tried to address the wafer scale GMR sensor/microfluidic integration issue using PMMA as the microfluidic material. The wafer scale integration of GMR sensor and PMMA microfluidic structures was almost realized, but the effort was given up at some point due to the complex integration procedures. For instance, in order to bond PMMA to Si, a metal layer, such as Ti or Au [3], is needed to enhance the bonding strength and, it may

bring side effects on sensor performance. Later on, we found that SU-8 has the advantage because it can be patterned by UV lithography and SU-8 fabrication processes are compatible with standard procedures for GMR fabrication at NVE. In addition, strong bonding between SU-8 and various materials can be achieved through a low temperature process to form sealed microfluidic structures [4].

The new fabrication process for microfluidics that integrates the GMR sensors on a wafer scale is shown in Figure 1. This process is developed based on previous work [5 6, 7]. A key component of this newly developed technique is the transfer of an uncured SU-8 layer from a sacrificial flexible substrate to the top of the patterned SU-8 structures. This layer serves for both sealing and interconnecting purposes. It is a novel and significant development in microfluidic field because it not only improves the yield of bonding area by using flexible substrate in stead of a rigid substrate such as quartz or glass used in [5], but also allows the multilayered structures, such as the fluidic interconnects, to be constructed on top of the uncured SU-8 layer after the sacrificial substrate is removed. Moreover, the fabrication is easy, because only aligned UV lithography is involved in building thousands of interconnects to the buried microfluidic channels, which has advantageous over the previous work [7] because it eliminates the drilling of interconnects from a hard material such as plastic or glass substrate. This turned out to be extremely useful in terms of wafer scale integration of microfluidic structures with GMR sensors. On the contrary, one of the most recognized techniques for integrating microfluidic developed by a group at MIT [5] will fail on wafer scale integration

1) Spincoat SU-8 on GMR wafers

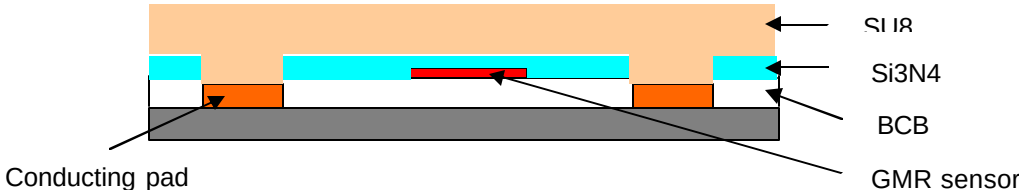

2) UV pattern SU-8

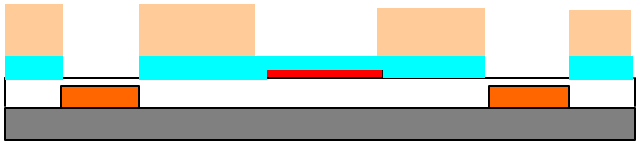

3) Prepare 2nd SU-8 layer on a flexible substrate

4) Assemble two SU-8 layers

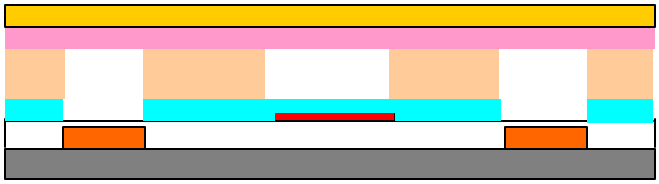

5) Remove flexible substrate and UV pattern SU-8 cover-layer for micro/micro interface

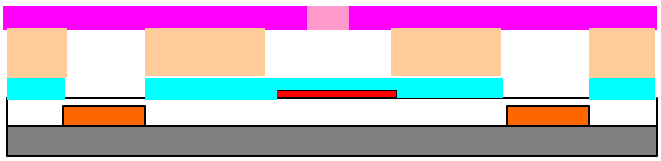

6) Dev SU-8 micro/micro interface holes

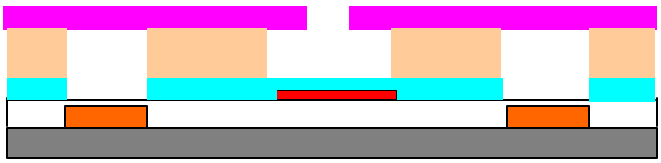

Figure 1. Process Design of Sensor/Fluidics Integration

The goal of our development is to put the microfluidic channels on top of the 4" wafer with GMR sensors fabricated from NVE. Since the wafer has some topography (~2μm) from the fabrication of the GMR sensor, a thin layer of SU-8 was used to flatten the surface before the channel layer was fabricated. Since there are as wide as 100μm channels and as narrow as 5μm channels at the same wafer, the exposure dose need to be controlled as precise as possible in order to realize the highest integrity of all the features.

After the microfluidic channels were fabricated, a flexible substrate (either Kapton or Mylar) coated with SU-8 resist was prepared as sealing layer. This sealing layer was soft-baked for a period of time to remove the solvent. The soft-back is critical to ensure the sealing of small channels without clogging. After soft-back, this SU-8 sealing layer was then brought into contact with the wafer bearing the GMR sensors and the SU-8 channels. Pressure was applied to ensure that there was large portion of contact area over a whole wafer and that air bubbles were eliminated. After bonding the SU-8 sealing layer to the SU-8 channel layer, the flexible substrate was removed and an aligned UV-exposure was carried out with an appropriate mask designed for the fluidic connects and dice space for each GMR sensor. After the post-exposure bake, the resist was developed to form the fluidic ports that connect the channels at the inlets and outlets. With this technique, we found that sealing of small channels ranging from a few micrometers in width was possible. Shown in Figure 2a is a sealed fluidic channel that is 10x10μm in cross-sectional dimension without evident seeping of SU-8 into the channel. A flow test by assembling the sensor/SU-8 unit with a PMMA chip connected to an external pump is shown in Figure 2b. to reveal the integrity of the SU-8 microfluidic unit. An additional advantage of the technique lies in that the thickness of sealing layer can vary within a range depending on the application.

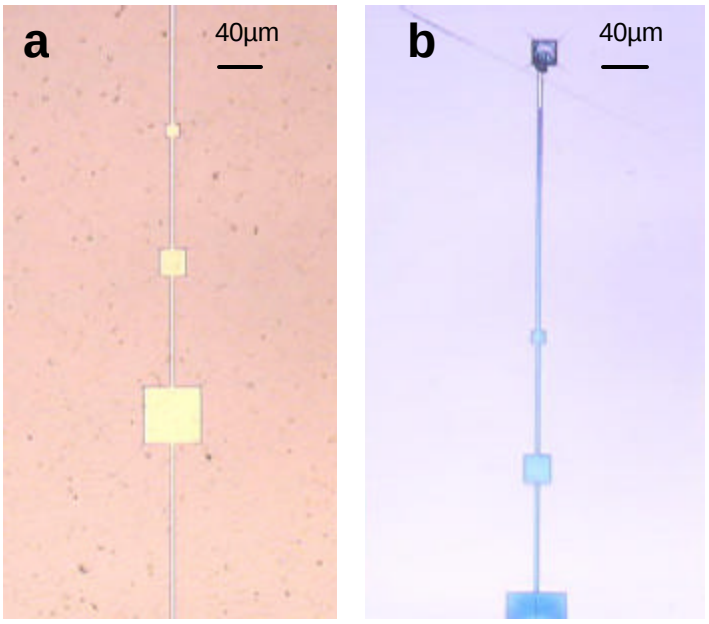

Figure 2. (a) Formation of sealed microfluidic channels with interconnects (the channels shown are 10µm in depth), and (b) liquid flow through without leaking.

Technical Results. An approach of integrating SU-8 microfluidic structures with GMR sensors on a wafer scale was developed based on multilayer SU-8 lithography and low temperature bonding. With this technique, we fabricated hundreds of sealed micro channels with thousands of interconnects on a 4" wafer that has hundreds of GMR sensors prefabricated (Figure 3). Fluidic channels with cross-section as small as 10x10µm have been sealed successfully. The integration process achieved a yield as high as 85% on a 4" wafer is possible. The results suggest that the microfluidic structures and GMR sensors can be integrated at wafer scale for mass production.

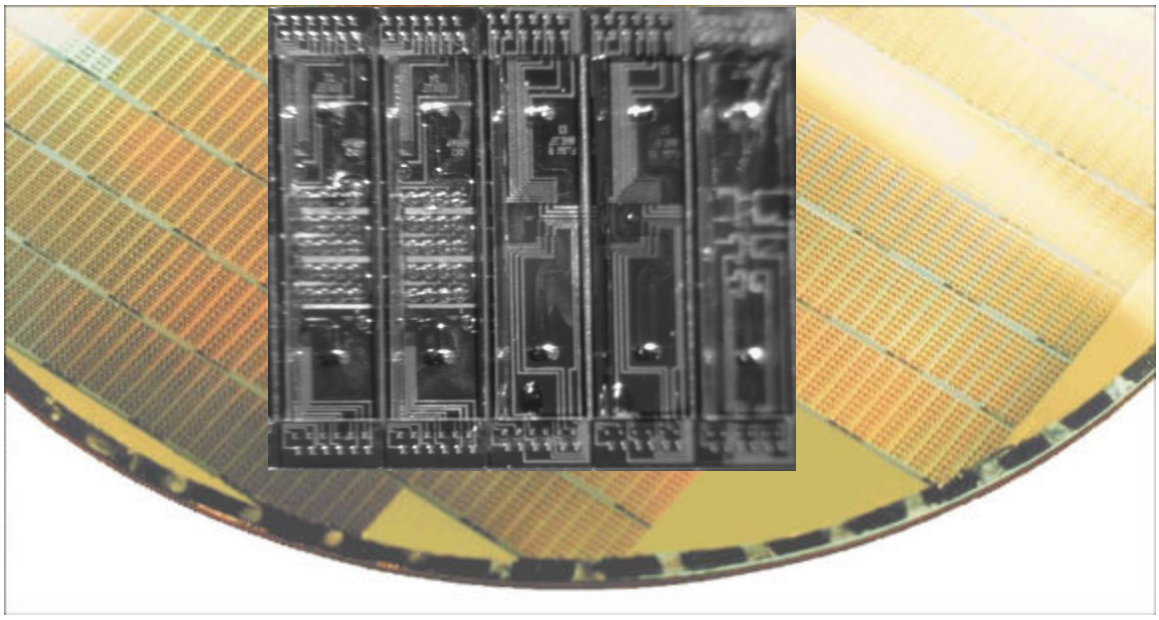

Figure 3. Wafer scale microfluidic/GMR sensor integration

2. Micro-Macro Fluidic Connectors

Technical Problems. The micro-macro fluidic interconnect is another critical components to make a microfluidic/GMR based assay system. The microfluidic system ensures that assay can be carried out in a fast, sensitive, and efficient way with tiny amount of sample required. However, standard micro/macro connectors will make microfluidic/GMR chip based assay become reality for field and inter-laboratories applications. A good micro/macro fluidic connector should have following characteristics: 1) no leaking, 2) low dead volume, 3) standard to share, 4) low cost for fabrication.

General Methodology. The GMR sensor platform for current BioMagnetICs project is shown in Figure 4, which is provided by NVE. The platform is a tee-shaped printed circuit board (PCB) with a wired bonded GMR sensor on it. The dimensions of this GMR sensor are about 1.5 mm by 6 mm with sealed microfluidic channels on top of it. The channel dimension values for current design vary from 15 μm to 100 μm. The diameter of the inlet and outlet is about 150 μm. The cover layer with patterned inlet and the outlet is about 40 μm in thickness, not strong and thick enough to support any tubing

connection. Also this PCB is designed to fit a excitation board with a exact plug-in position for measurement.

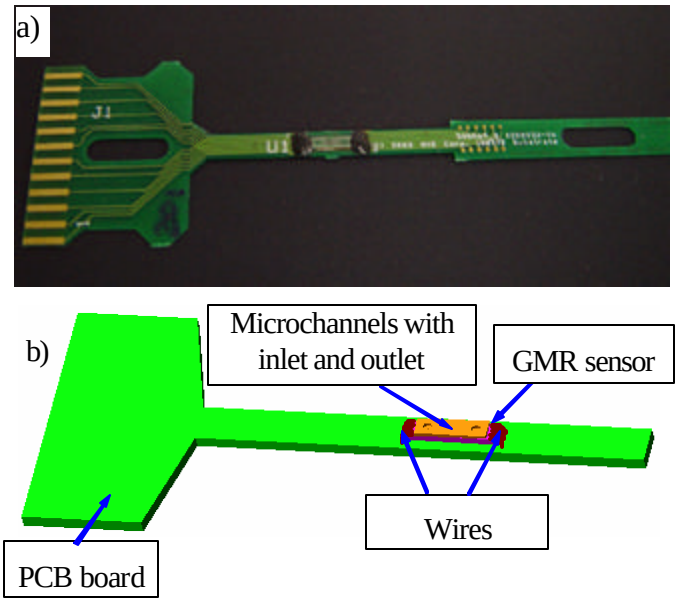

Figure 4. (a) A picture and (b) a 3D model of GMR sensors with PCB

Considering the above limitations, we design micro-macro fluidic connector, the GMR sensors, and the PCB as a whole unit. The connector module (see Figures 5(a) & 5(b)) consists of two components made from PMMA, which are made from CNC machine. One piece has tow standard 1/4”-28 thread tubing adapters and two micro channels at the bottom for connecting macro scale liquid to microfluidic structures. Another piece has PDMS pad adaptor with tow through holes that match the holes on GMR sensor surface. PDMS pas is used as sealing gasket to prevent leaking. When bonding the connector to the PCB, a compression force will press the PDMS soft pad to seal the connection holes. During the fabrication processes of connector module, two PMMA parts are integrated together by thermal bonding. The PDMS pad is molded with by using lithography patterned SU-8 molds.

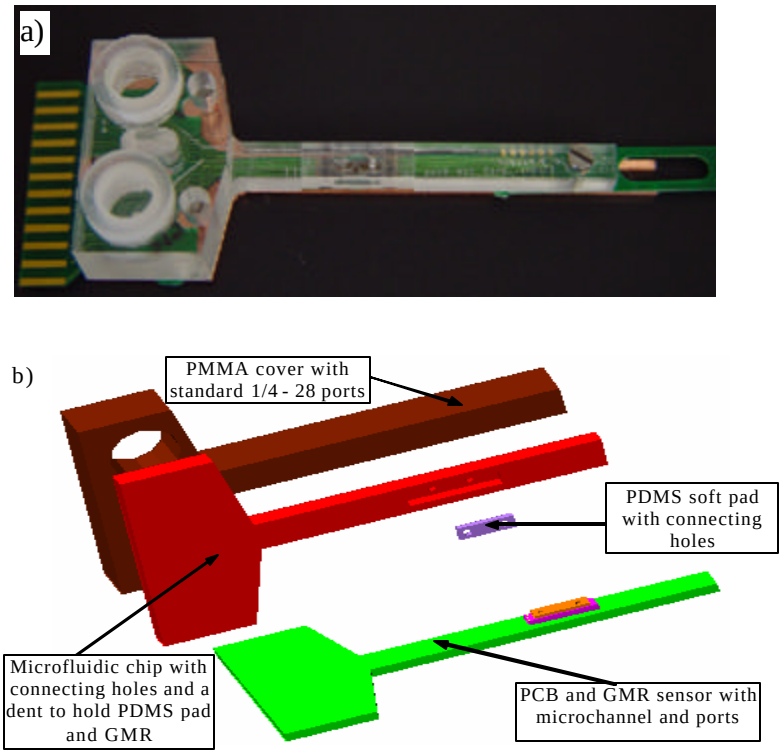

Figure 5. (a) assembly macro/micro connector with GMR sensor on PCB, and (b) 3D model of the fluidic connector for GMR sensor.

Technical Results. After assembly, the tests have been done and there is no leaking. Figure 6 shows the liquid flowing through the channels over the GMR sensors surface.

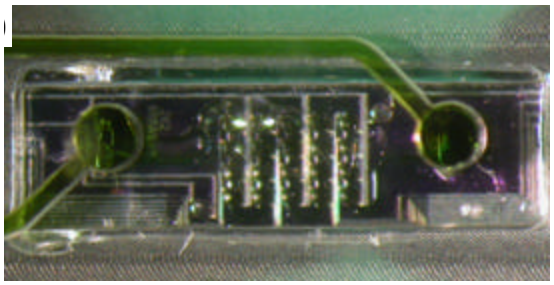

Figure 6. Fluid flowing through channels over the GMR sensors

The results show that this kind of micro/macro connector approach is easy to fabricate with relatively low cost. It also can be made by injection molding technique for massive production with integrated tubing connectors.

3. Development of Magnetic Nanoparticles with Improved Properties

Technical Problems. GMR based biosensors require magnetic nanoparticles with high magnetic moment in order to improve the sensitivity of detection. In addition to the magnetic moment, enhancement of magnetic properties such as blocking temperature, coercivity, saturation magnetization of the magnetic nanoparticles is also required. Magnetic properties of the nanoparticles are strongly influenced by the presence of organic as well as inorganic protective shells on their surface. Taking advantage of this, we have begun a systematic investigation to design new cobalt-based magnetic nanoparticles with improved magnetic properties by varying the magnetic core and its size, protective metallic shell and its thickness and chemical nature of the stabilizing agent.

General Methodology. Cobalt nanoparticles encapsulated by an antiferromagnetic shell has been recently reported, pushing the superparamagnetic limit to nearly room temperature. In addition, without a protective shell, the utility of Co nanoparticle is limited due to its propensity for oxidation. To date, the use of a noble metal shell, such as gold, platinum, and insulating shells such as SiO_2 have been demonstrated.

An electroless method was developed to fabricate Co@Cu (or Au) core-shell nanoparticles. The direct reduction of copper (or gold) ions with cobalt without the need for a reducing agent was carried out for generating the core-shell particles. The facile oxidation of the cobalt nanoparticle dictates that the cobalt oxide be removed before the shell synthesis, or that it be avoided altogether. Both approaches are presented here for Co@Au and Co@Cu, respectively. The Co@Au nanoparticles were synthesized in N_2 protection in order to prevent the oxidation of the cobalt core during the gold shell formation in an organic THF medium. The dissolution of the cobalt oxide in acidic electrolytes is a new approach taken, that eliminates the need to keep the nanoparticles in an inert environment. This method is demonstrated for the synthesis of Co@Cu core-shell particles.

A wet chemical reduction method was used to obtain Co nanoparticles with 3-(N,N-dimethyldodecylammonio)propanesulfonate (SB12) as the surfactant, to prevent agglomeration, and lithium hydrotriethyl borate ($LiBEt_3H$, superhydride) as the reducing agent, Eq. (1).

$$CoCl_2\text{-SB12}+LiBEt_3H \rightarrow \mathbf{Co}(\text{nanoparticles})\text{-SB12}+BEt_3+LiCl+H_2? \quad (1)$$

An organic solvent, tetrahydrofuran (THF), was used instead of water to avoid oxidation. In the case of the Au shell, the electroless scheme took place directly in the THF solvent.

$$KAuCl_4 + Co_x\text{-SB12} \rightarrow \mathbf{Co\text{-}Au}\text{-SB12} + KCl \qquad (2)$$

The copper shell was formed in an aqueous copper citrate solution, at pH=4.

$$Co_x\text{-SB12} + Cu^{+2} \rightarrow \mathbf{Co_{x-1}\text{-}Cu}\text{-SB12} + Co^{+2} \qquad (3)$$

Technical Results. The magnetic properties were characterized using a SQUID magnetometer (Quantum Design MPMS-5S) and the structure was observed by TEM (JEOL model 2010).

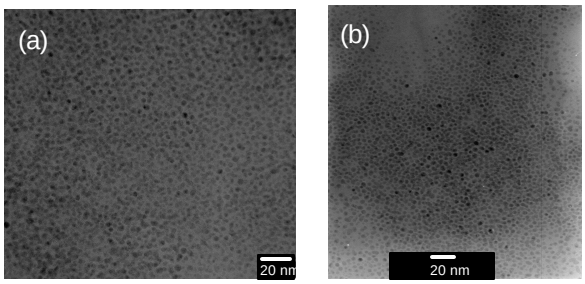

Figure 7. TEM image of (a) Co@Cu core-shell NPs, and (b) Co@Au nanoparticles

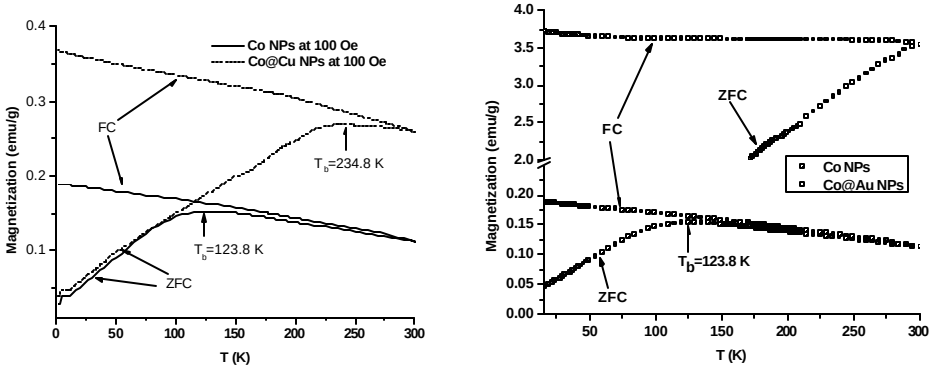

Figure 8. ZFC and FC magnetization at an applied magnetic field of 100 Oe for (a) Co@Cu, and (b) Co@Au core-shell nanoparticles.

Monodisperse Co core-shell nanoparticles were observed, shown in Figure 7. Both the zero field cooled (ZFC) and the field cooling (FC) conditions were measured (Figure 8). The blocking temperature, T_b, was found to increase from 123.8 K, to 234.8 K and to greater than room temperature for Co, Co@Cu and Co@Au NPs, respectively. Characterization of the shell stability was also examined. The Co@Au NPs were exposed to air and immersed in aqueous HCl solution, pH=2 for 3 hours. The stability was monitored by measuring the magnetic property.

4. GMR Circuitry Optimization for High Sensitivity and High Resolution Measurements

Technical Problems. It is great jump start to use NVE GMR sensor excitation/data acquisition (DAQ) board for assay system integration. As the current goal is to achieve few to single Dynal beads detection on GMR sensor surface, a signal as small as 1μV needs to be measured. The conventional 16 bits DAQ is not sufficient for this kind application because even used in a range of +/- 0.5V only a 15μV resolution can be achieved. Besides the high resolution requirement for DAQ, a high current supply for Wheatstone bridge excitation is also needed. If it is necessary, a modulation signal can be used to change the in plane magnetic field for lock-in detection. At current time, a system with all aforementioned features is not available and a testing station has been set up to conduct tests in variety of ways.

In order to achieve quantitative measurement from the GMR sensor, sensor calibration is essential. The testing probes with variety numbers of Dynal beads on them are needed. These probes have to provide a means to let magnetic beads have a close contact with the GMR sensor surface and will not contaminate the surface so that the repeatable testing can be conducted on a identical condition without introducing extra variables. Polymer based micro probes with fixed number of Dynal beads on each of them have been developed and used as standards for GMR sensor system calibrations.

General Methodology. Using several external instruments we are able to configure the test station in a variety of ways. The sensor signal is filtered by low-pass filter to block 60 Hz noise and its harmonics and amplified by instrumentation amplifiers prior to digitization. An IC micro probing station is used as a basic platform for testing station. It not only allowed us to probe the sensor surface with accurate position control, but it also afforded us the ability to use its microscope and CCD camera to align the probe over the sensor surface as well as visually document experiments. An extra shielding was added to the GMR sensor along with signal conditioning circuits closer to it, which can further reduce noise injected into system from environment. A computer controlled precision external power supply is built for supplying the current to the GMR Wheatstone brides with accuracy down to pA range. A modification has been made to modulate the

in plane magnetic field in order to use lock-in detection, see Figure 8 for testing station set-up flow chart.

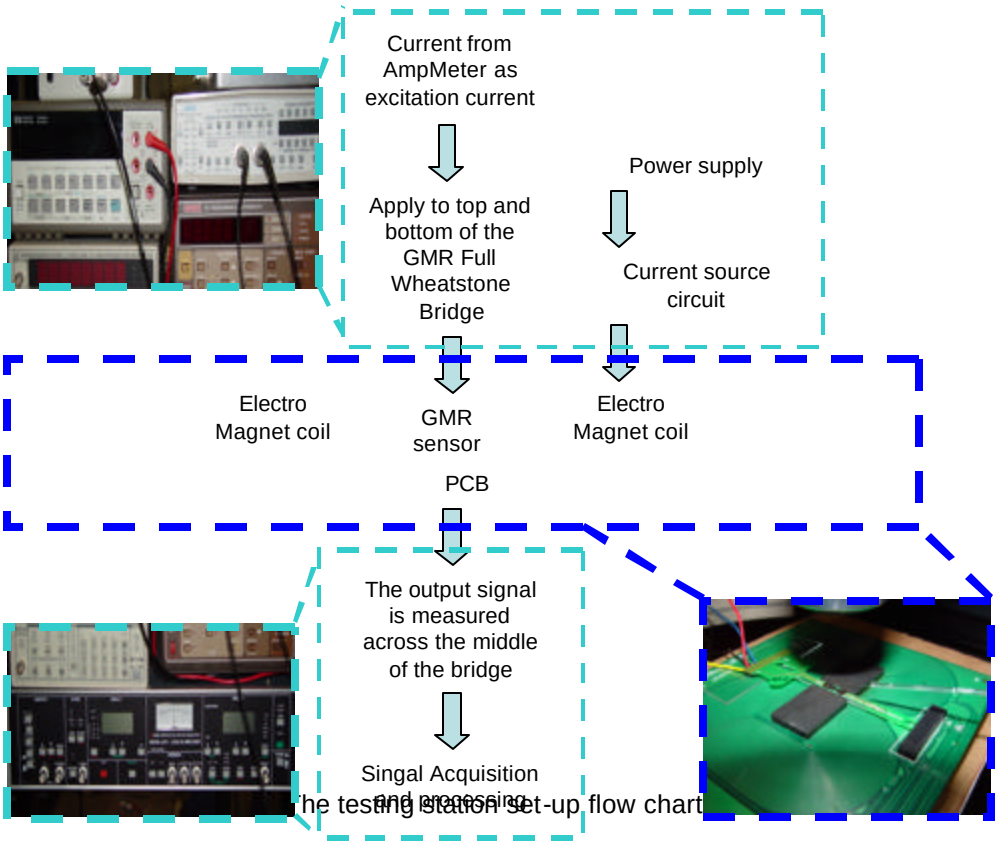

The testing station set-up flow chart

The first generation of probes was made from drawn glass fibers. These fibers were then glued into the end of micro pipettes. A specific number of beads were attached to the end of the fibers. The micropipettes were slightly bent to the proper angle to fit the micro probe manipulators. Fiber thickness ranged from ~3µm to ~100 µm.

The second generation of probes was made by micro lithography technique. A monolayer of Dynal beads is formed on a substrate, which is then coated with 1 µm thick SU-8 photo resist to fix the beads together. The individual 200 μm^2 tips with specific numbers of beads embedded in the SU-8 were patterned and the tips are then mounted on levers to be used for probing in the micro manipulators. Figure 9 shows the partial area of the tip.

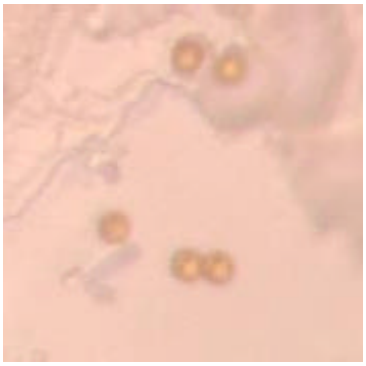

Figure 9. Dynal beads embedded inside the SU-8 patterned probe tip

The probes are then used to characterize each GMR sensor for its response to a known number of micro beads. The probe can be dropped to the GMR sensor surface and removed away in a controlled manner without surface contamination. Therefore, the downtime between system reconfiguration is greatly reduced and more repeatable, accurate calibration can be obtained.

Technical Results.

The GMR module from NVE has been tested using the testing probe with about 100 Dynal beads (2.8 μm in diameter). The excitation signals and data acquisition were performed by CAMD testing station. Testing results show that with current set up, the signal from our testing probe (about 100 beads) is around 100 μV, the detection limit is about 100 Dynal beads with a signal to noise ratio of 20 db (figure 10).

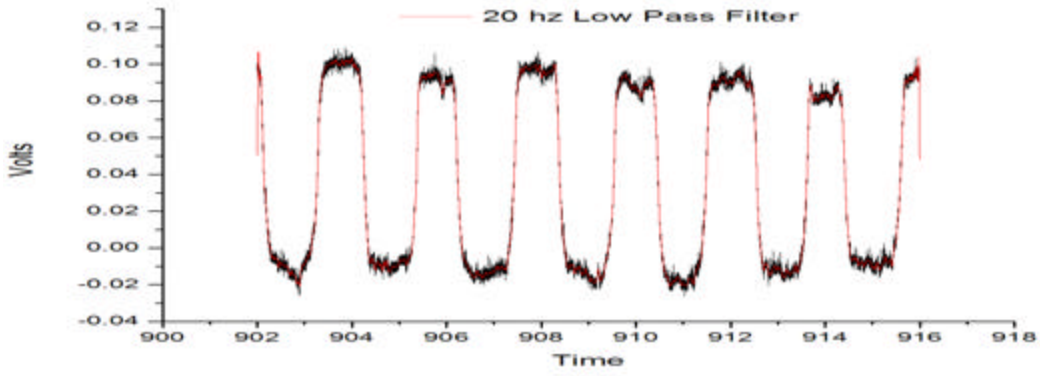

Figure 10. Signal generated from NVE GMR sensor by ~100 2.8 μm Dynal beads .

5. Sensor and Magnetic Particles Surfaces Functionlization for High Sensitivity and Specificity Assays.

Technical Problems The ultimate goal is to produce a relevant bio-active surface patterned on GMR sensor pad during manufacturing, sealed within fluidic channel, capable of surviving elevated temperatures, dryness, and organic solvents while producing the desired final bio-assay results.

Creating a bio-functionalized sensor surface that can withstand the rigors of sensor manufacturing, long-term storage, while preserving the desired biological properties is a very complex problem. There are a number of "unique" challenges in addition to the "normal" bio-assay challenges. "Normal" demands encountered while creating a bioassay with a new sensor system include: high specificity, good dynamic range, low background signal, reproducibility, and multi-analyte detection/analysis. The "unique" challenges arise from the manufacturing processes that imposes constraints of high temperatures, dry surfaces, organic solvents, blocked surface access, and wafer scale processing. Finally the requirement for long term storage of bio-functionalized surfaces and bio-reagents produces a different set of constraints. The below table summarizes some of the major design boundary conditions.

Table 1: GMR Bio-Interface Boundary Conditions

Category	CAMD Real World Environment
Surface Selection	Dictated by Sensor Surface Material
	Impacted by Manufacturing process
	Limited by Fluidics
Assay Protocol	Few number of reagents available
	Limited reagent volumes
	Storage tolerant reagents
	System Threshold Considerations
Manufacturing	Elevated Temperatures
	Dry Surfaces
	Organic Solvents
	High throughput Production with QC
Extended Storage of Surface and	Temperature Stable

Assay Reagents	Time Stable Predictable degradation Behavior
Patterning	Sever Feature size / resolution require. High Throughput Production Wafer Scale compatible Sealed Fluidic Channel

General Methodology. CAMD's Bio-Interface approach to this problem has been to create a multi-layer structure, with each layer withstanding the rigors of that step of manufacturing, while at the same time enabling the next step of manufacturing, bio-functionality, or storage.

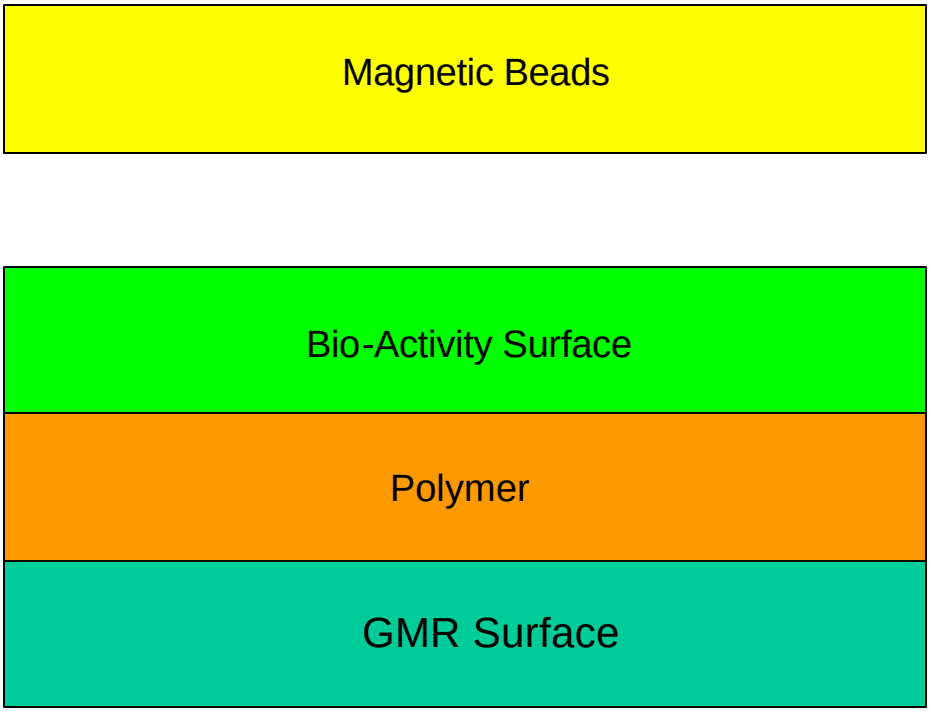

Figure 11. Functionality via Layers

Each layer of the structure provide a specific set of characteristics to the final GMR sensor system. The polymer is necessary for manufacturing and long term storage. The bioactive surface is necessary for assay specificity and target recognition and retention. The magnetic beads are necessary to generate a signal from the GMR sensor.

Technical Results

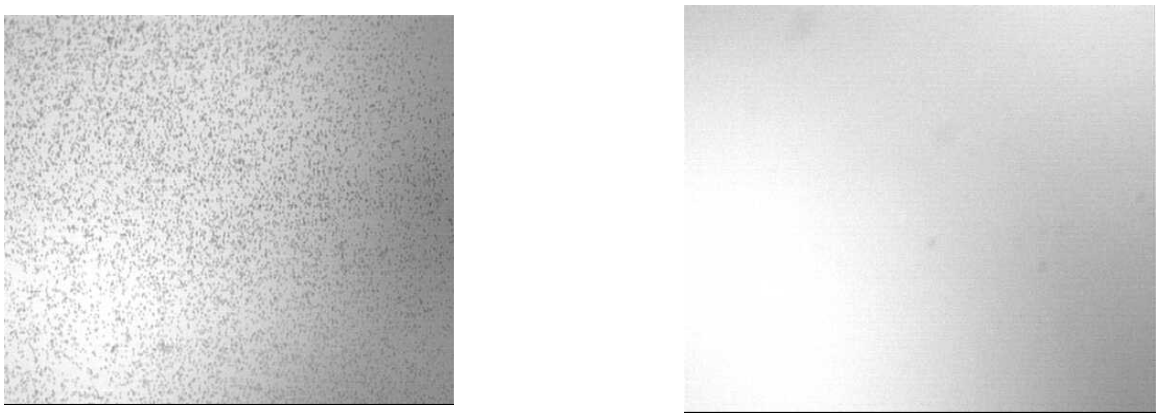

BioAcitve

Background

Figure 12. Manufacturability

Manufacturability is critical for high volume production sensor systems.. The panels shows magnetic bead binding to bio-active surfaces that can be dried for greater than 90 minutes, and heated to 60C for greater than 20 minutes. Left panel show binding to the bioactive surface and right panel shows background binding.

Glass

Polymer

Bioactive

Figure 13. Low background Binding

Low background binding is essential for good signal to noise ratios, assay sensitivity, and limit of detection. Far left panel shows magnetic bead binding to glass. Middle panel shows magnetic beads binding to polymer layer. Far right panel shows magnetic beads binding to the bio-active surface.

Bioactive 1 mm

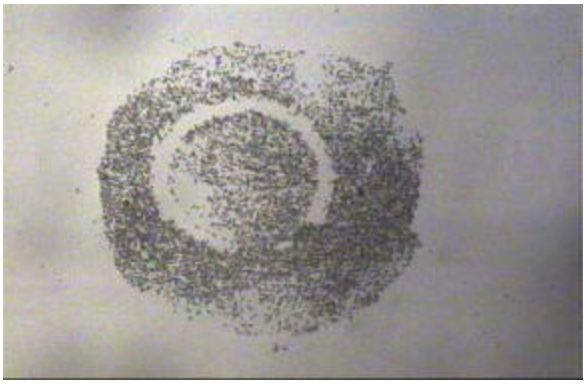

Bioactive 400 um

Figure 14. Bioactive Patterns on Glass

Patterning the bioactive surfaces places the magnetic signal directly over the GMR sensor pad and off the GMR reference pads. Left and right panels show magnetic beads binding to bio-active surfaces that were patterned by two different techniques. These initial bio-active surfaces were patterned "by-hand".

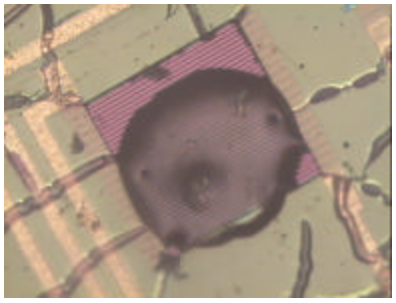

GMR Pad 200 um

Figure 15. Pattern on GMR surface

Ultimately patterning of the bioactive surfaces must be computerized and be scalable to "whole wafer" processes. This panel shows a polymer layer patterned on the sensor pad of the GMR sensor by such equipment. Sensor pad is 200um square.

Figure 16 Protein Toxin Assay

Target specificity and limits of detection are two of the critical factors necessary to the ultimate functionality of the GMR sensor. Shown to the left are the results of a sandwich assay using magnetic beads for the detection of protein toxin stimulant, ovalbumin at three concentrations.

Future research will focus on consolidating the above features of manufacturability, low background, patterning, wafer scale, and protein toxin assay into a single location coincident with the GMR pad encapsulated within a sealed micro-fluidic delivery system.

SUMMARIES AND COMMENTS

1. There is a significant achievement on wafer scale microfluidic/GMR sensor integration with a reasonable yield rate at prototype stage. This integration technique is compatible with the GMR sensor fabrication and packaging techniques, which may result in a commercially available microfluidic/GMR chip for different applications. The fabrication procedures and techniques need to be optimized for better quality control and high yield.
2. A micro/macro fluidic inter-connector module has been designed and fabricated, which provides a standard liquid interface connecting the macro liquid world to microfluidic chips. This kind of connecting module can be made from injection molding technique for massive production with low cost. The second generation inter-connectors that will use LiGA technique for more accurate dimensional control and cost reduction is under the development.

3. Nanoparticles with higher magnetic momentum have been developed at CAMD, which make one step closer to the single particle detecting using GMR as sensor. The functionlization of these nanoparticles will be one of the key objectives for coming project research and development.
4. A GMR/microfluidic testing station has been established at CAMD for GMR sensor calibration and signal measurement. Transfer current set-up to a hand-held system is one of the next goals for this project.
5. Sensor surface fictionalization produced by CAMD Bio-Interface has demonstrated a solution that satisfies many of the complex criteria of the manufacturing a GMR bioactive surface including: withstanding hot/dry manufacturing conditions, low background binding, patterning, wafer scale, and initial sandwich assay of protein toxin stimulant. Future research will focus on consolidating the above features into a single location coincident with the GMR pad encapsulated within a sealed micro-fluidic delivery system.

References

1. Schjolberg-Henriksen K, Plaza J A, Raft J M, Esteve J, Campabadal F, Santander J, Jensen G U and Hanneborg A, 2002, Protection of MOS capacitors during anodic bonding, *J. Micromech. Microeng.,* **12**, 361-367.
2. C. R. Tamanaha, L. J. Whiteman, and R. J. Colton, "Hybrid macro-micro fluidic system for a chip-based biosensor", *J. Micromech. Microeng.*, vol. 12, pp. 7-17, 2002
3. K. F. Lei, W. J. Li, N. Budraa, and J. D. Mai, "Microwave bonding of Polymer-Based Substrates for Micro/Nano Fluidic Applications," *The 12th Intl. Conf. on Solid-State Sensors, Actuators and Microsystems (Digest of Technical Papers)*, pp.1335-1338, 2003
4. C-T. Pan, H. Yang, S-C. Shen, M-C. Chou, and H-P. Chou, "A low-temperature wafer bonding technique using patternable materials," *J. Micromech. Microeng.*, vol. 12, pp. 611-615, 2002
5. R. J. Jackman, T. M Floyd, R. Ghodssi, M. A. Schmidt, and K. F. Jensen, "Microfluidic systems with on-line UV detection fabricated in photadefinable expoxy", *J. Micromech. Microeng.*, vol. 11, pp. 263-269, 2001
6. J. Carlier, S. Arscott, V. Thomy, J. C. Fourrier, F. Caron, J. C. Camart, C. Druon and P. Tabourier, "Integrated microfluidics based on multi-layered SU-8 for mass spectrometry analysis", *J. Micromech. Microeng.*, vol. 14, pp. 619-624, 2004
7. Y. Song, C. Kumar, and J. Hormes, "Fabrication of an SU-8 based microfluidic reactor on a PEEK substrate sealed by a 'flexible semi-solid transfer' process", *J. Micromech. Microeng.*, vol. 14, pp. 932-940, 2004

PART 3 – LSUHSC Report

Bio-Magnetics Interfacing Concepts: A Microfluidic System using Magnetic Nanoparticles for Quantitative Detection of Biological Species

(Subcontractor: LSUHSC)
Neuroscience Center of Excellence
Louisiana State University Health Sciences Center
2020 Gravier Street, Suite D
New Orleans, LA 70112-2234

LSUHSC – DARPA BioMagnetics Project

Project 1: Head Injury.

1. Task Objectives

The main interest of LSU-Neuroscience Center researchers is to study neurochemical mechanisms of brain injury that are of great interest to the military. The final objective of this project is to fill major gaps in our knowledge as to which molecular and cellular mechanisms are critical for the selective brain vulnerability that is impaired in mild traumatic head injury (MTHI) consciousness. We will make use of the magnetic nanoparticles technology that will be developed in CAMD and/or AMRI to explore 1) a more efficient delivery of neuroprotectant drugs, 2) signaling mechanisms leading to neuronal cell death and 3) ways to prevent undesirable degrading mechanisms due to injuries.

To that end, we will use two main experimental models: a*) in vivo*: The fluid percussion head injury (FPI) model will be used to reproduce traumatic brain injury (TBI) in the rat, to follow biochemical, histological and behavioral. Characterization of this TBI model is the first step for the evaluation of neuroprotection by new drugs that eventually will be complex to nanoparticles for a more efficient delivery and a faster action.

b) *in vitro*: To develop cellular biomagnetics tools to investigate brain cell signaling and cell injury. There are two objectives: 1) Development of magnetic particles to aid in particle visualization and optimization of cell interaction for cell signaling and drug delivery; 2) Development of a magnetic microscope probe to aid in control of particle cell interaction and drug delivery. These series of studies were done under Dr. Mark DeCoster's supervision.

2. General Methodology

***Fluid percussion injury*:** *In vivo* TBI triggers an inflammatory cascade that results in increased blood brain barrier (BBB) permeability, edema and infiltration of leukocytes leading to neuronal cell death. Wistar rats (250-300g body weight) were anesthetized with halothane, and a 4 mm craniotomy was done on the right parietal cortex. A 2 mm female union-bolt was cemented to the skull and animals were left to recover for 24 hours prior to the FPI (3 atm., 100 ms duration). Animals were left for different periods of time, up to 7 days with food and water *ad.lib.* BBB permeability was evaluated at 24, 48 and 72 hrs after FPI by measuring Evans blue dye extravasations.

Histopathological analysis. Apoptotic cell death was investigated by TUNEL in paraffin sections (Gavrielli et al., 1992), using terminal transferase-mediated biotinylated d-UTP nick-end labeling. Immunohistochemical detection of glial fibrillary acidic protein (GFAP), and mieloperoxidase (MPO) was done in deparaffinized and rehydrated sections blocked with 10% normal goat serum for 1h to overnight and GFAP-CY 3 conjugate (1:100) or rabbit anti human MPO (1:100), respectively. The Deconvolution Imaging System was used for analysis and imaging.

***In vitro studies*:** Our working model utilizes primary cell cultures of rat brain cells as well as a human umbilical vein endothelial cells (HUVECs). Using these cells in various cell culture dishes and plates allows us to monitor by microscopy magnetic particle-cell interactions both acutely and long-term. We have constructed an electromagnetic probe

for our microscopy imaging system, which is positioned in all 3 axes with a manual micromanipulator. In synthesizing fluorescent magnetic nanoparticles, we have used streptavidin-labeled with Alexa 546 (red) to aid in visualization of the particles under the microscope. Acute control of particles is controlled by a variable electromagnetic microscope probe, which we have constructed. Long-term control of particles utilizes a permanent magnet available from Molecular Probes (Invitrogen).

3. Technical Results

***In vivo studies*: TBI.** The level of Evans blue recovered from the damage (right) hemisphere was increased 3.9-and 5.0-fold at 24 and 48 h, respectively, while in the contralateral hemisphere these values were 3.3-and 2.4 fold, indicating a lower, although significant, alteration of the BBB and a faster recovery than in the damage site (**Figure 1**).

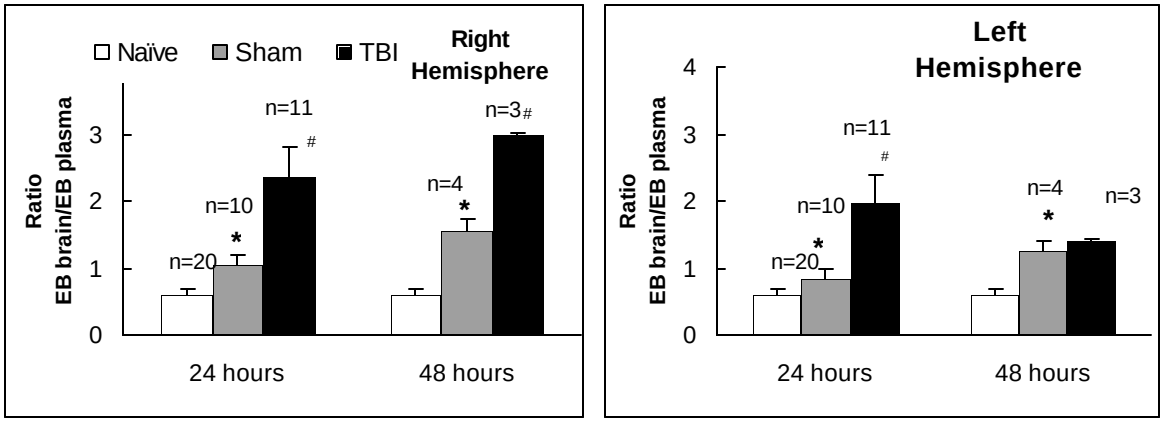

Figure 1. Alteration in BBB permeability 24 and 48 hours after FPI.
Mean values + SEM from the number n of individual determinations are shown.
*, p< naïve; #, p< Sham (Student's ttest p< 0.05)

Histological examination by Tunel 48 hrs after trauma showed the area of apoptotic cell death and by 7 days reactive gliosis was detected with GFAP in the FPI area (**Figure 2 and 3**) . All studies were done in parallel in sham control animals.

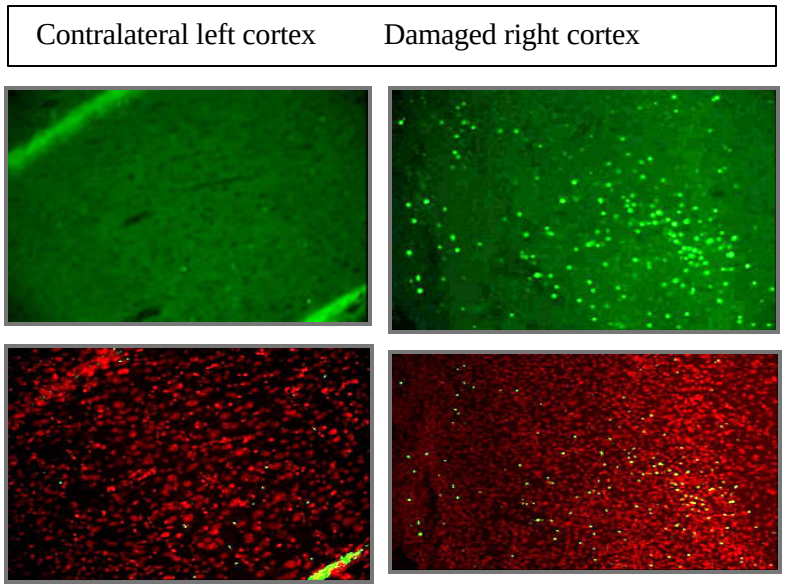

Figure 2. TUNEL allow detecting damaged neurons with DNA fragmentation in the damage hemisphere.

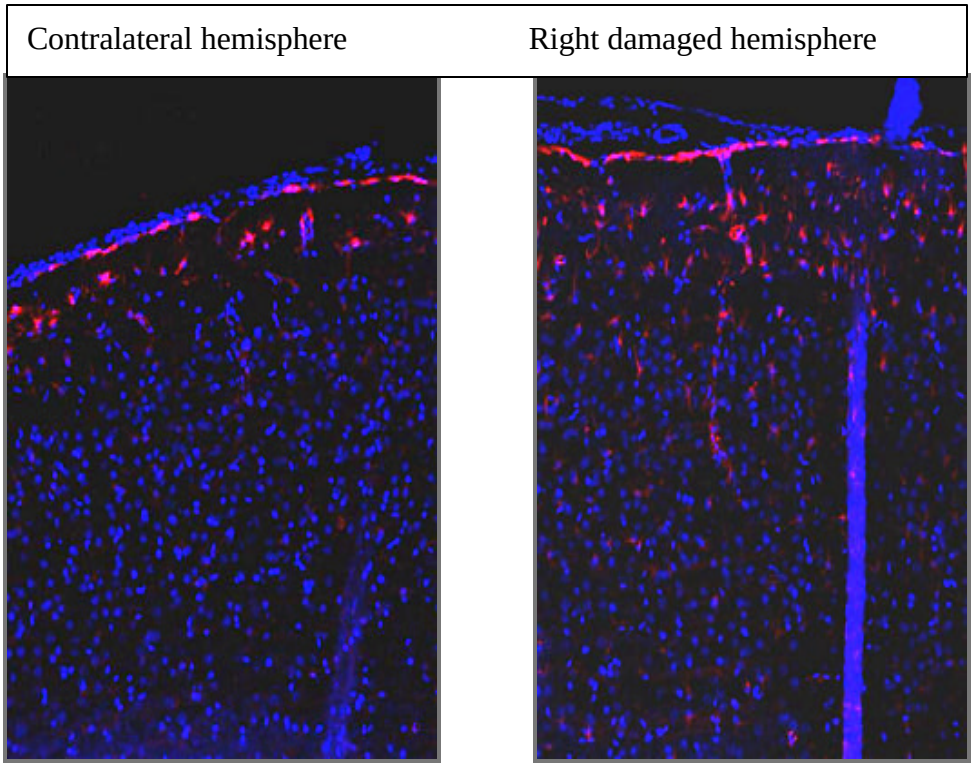

Figure 3. Reactive microglia can be observed bellow the area of FPI, and may contribute to the expansion of the infarction

***In vitro studies*.**

1) In collaboration with CAMD, we have synthesized fluorescently-labeled streptavidin bound paramagnetic particles.

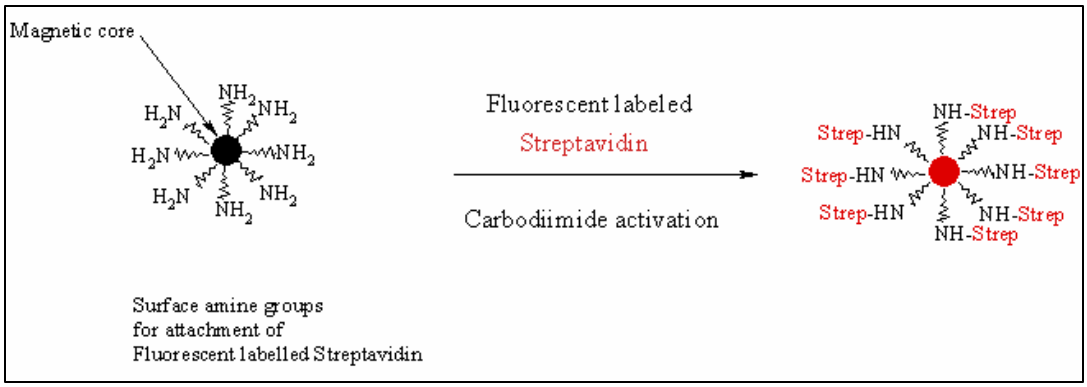

Figure 4. Fluorescently labeled streptavidin (Alexa 546) was bound to amine groups on magnetite nanoparticles. This synthesis strategy will allow us to potentially link biotin-labeled proteins or drugs to the streptavidin magnetic particles, for use in cellular and tissue targeting.

We are able to visualize the particles under both phase light and fluorescence. We can control the fluorescent particles with a magnetic field.

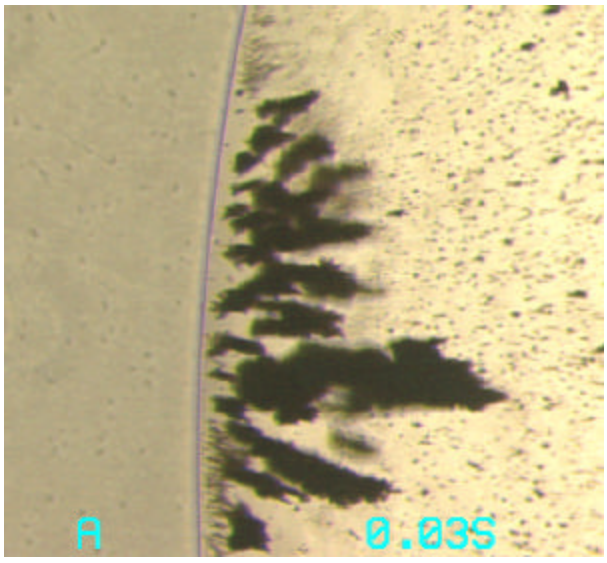

Figure 5. Particles coated with a drug (SCP-22) are much larger and clumped compared to the uncoated particles, but the magnetic probe is still able to control and orient these larger clumps.

2) We have constructed a useful variable electromagnet that can be positioned with a micromanipulator to image probe-particle interactions and interactions with cells using an inverted microscope.

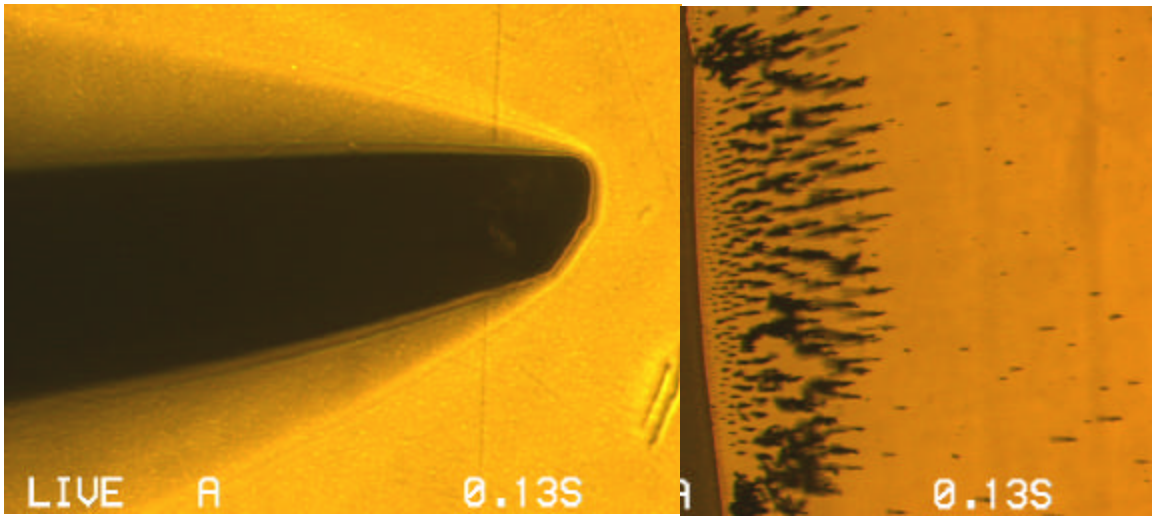

Figure 6. The magnetic probe was positioned with a micromanipulator down to the plain of focus of the microscope, showing the tip of the probe. Larger, 2 µM paramagnetic particles from Polysciences, suspended in liquid, are oriented by the magnetic probe, positioned outside the liquid to the left.

3) We have successfully interacted magnetic nanoparticles with primary cultures of rat neurons and astrocytes. These magnetic particles can be positioned for days at a time with a permanent magnet. We found that magnetic particles appeared to interact better with astrocytes than with neurons

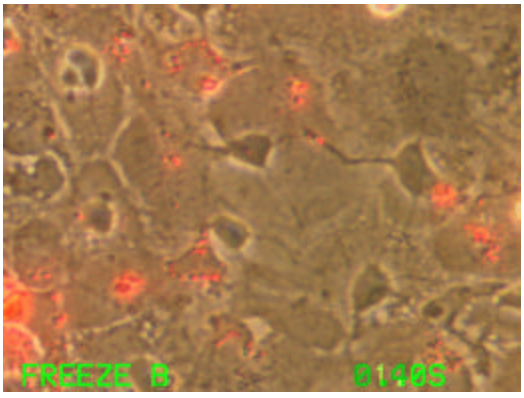

Figure 7. Nanometer-sized paramagnetic particles from CAMD were combined with mixed cultures of neurons and astrocytes from the brain. Particles were linked to streptavidin and Alexa 546, and thus appear red in this merged phase+fluorescence image. While we found no specific association with neurons, astrocytes appeared to bind or internalize the particles.

However, no cytotoxic effects of long-term particle-cell interaction were observed.

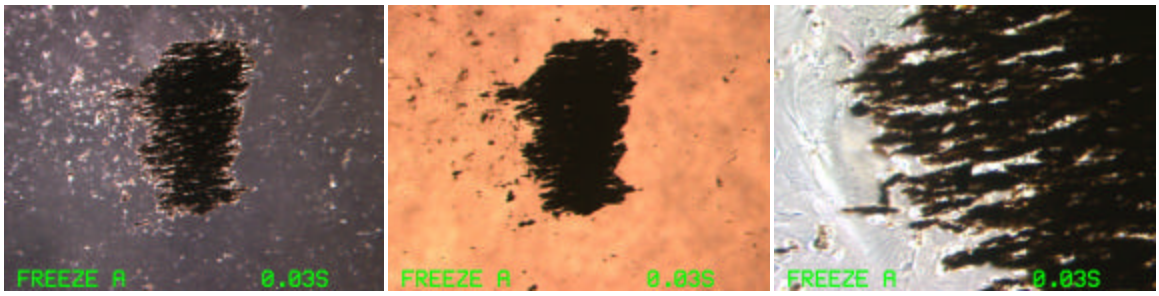

Figure 8A. Primary cultures of astrocytes from rat brain were interacted with paramagnetic particles for 1 day in vitro, and then placed on a permanent magnet (Molecular Probes). After one day in vitro on the permanent magnet, large organized arrays of particles were observed in the middle of the magnetic field. 4A+B, 20x magnification, 4C, 100x magnification.

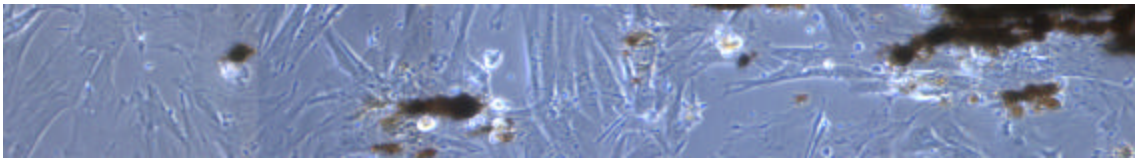

Figure 8B. A mosaic to the left of the magnetic array showing possible alignment of astrocytes towards the magnetic field.

4. Importance of findings and Conclusions

1- FPI is an excellent model that we plan to use in the near future to test the therapeutic effect of new drugs delivered attached to biomagnetic nanoparticles. *In vitro* studies with brain cells in culture have allowed us to develop a fluorescent streptavidin-labeled magnetic particle that associates with cells, and we have also developed a magnetic microscope probe that allows us to better control position and association of the particles in relation to the cells of interest. These developments may aid in delivery of potentially neuroprotective drugs in the short term *in vitro*, and ultimately, *in vivo.*

2- In collaboration with CAMD we have successfully constructed fluorescent, streptavidin-labeled superparamagnetic nanoparticles that adhere to astrocytes from the brain. This adherence has allowed us to investigate particle-cell interaction with the aid of a magnetic microscope probe which we have constructed. Attachment of these magnetic particles to living cells may be used to investigate in the future, stress initiated signal transduction such as calcium influx.

3- We have demonstrated in two cell culture models, effects of long-term interaction of cells with magnetic nanoparticles. In brain cell cultures, particles interact mainly with astrocytes, and we have also demonstrated cell interaction with particles using HUVECS. These long-term studies

will be important for investigating possible long-term side effects of particles in association with cells, which needs to be determined for further development of particle-based drug delivery. While primary brain cell cultures will serve as an excellent model for investigating cell signaling and injury in the brain, the HUVECs culture model will be a more straightforward system for investigating development and delivery of anti-inflammatory drugs of potential therapeutic interest.

5. Technical problems encountered

1. We have constructed fluorescent streptavidin-labeled superparamagnetic nanoparticles in collaboration with CAMD. While useful in that these particles retain superparamagnetic properties and some fluorescence, we encountered problems with these particles clumping and aggregating after functionalization (after addition of the fluorescent streptavidin), in comparison with starting particle material. In addition, labeled particles were not uniformly fluorescent, and many were only weakly fluorescent as determined by microscopy.
2. We have constructed a variable electromagnetic microscope probe for controlling particle-cell interactions and drug delivery. In our initial prototype the dissecting pin used to construct the probe, while useful in size and length, retains magnetic properties after removing the electrical current to the probe. More useful would be a probe that does not have magnetic memory.

6. Implications for further Research

1. Further development of fluorescent streptavidin-labeled magnetic nanoparticles will aid in investigating particle-cell interactions, which can then be further controlled by a magnetic field. Areas include cellular effects of long-term magnetic fields and effects of mechanical stress on cells.
2. Particle cell interactions will be important for defining further development of particle based drug delivery. This will include defining possible side effects of long-term particle association with cells, and efficiency of particle adherence/uptake by cells.
3. Development of better magnetic microscope probes will aid in potentially focusing and controlling particle location for drug delivery, and will also allow for visualizing and invoking mechanical stress or other stimulus to living cells in culture.

7. Lectures and Posters presented under this project

At DARPA Mardi meting at the Marriott Hotel in New Orleans, LA, 19 February 2004:

1. Lecture: "Neuronal Cell Signaling and Sensing using Magnetic Particles" Mark A. DeCoster
2. Poster: "Fluid percussion: experimental model of traumatic brain injury". E. B. Rodriguez de Turco, A. Waldren, J. Ramirez, K Van Meeter, J. Moses and N. G. Bazan

Lectures and Posters presented under this project at the Louisiana Consortium BioMagnetICs Quarterly Review meeting at the Center for Advanced Microstructures and Devices (CAMD), Baton Rouge, LA, 18 August 2004:

1. Lecture: "Update on Biomagnetics Neurobiological Studies" Mark A. DeCoster, PhD.
2. Lecture: " Strategies for developing neurorestorative approaches using biomagnetics" Elena R. de Turco, PhD
3. Poster: "Development of a magnetic microscope probe for controlling particle-cell interaction" M. A. DeCoster and N.G. Bazan.
4. Poster: "Synthesis of fluorescent paramagnetic particles as biomagnetics tools" M.A. DeCoster, C. Kumar, J. Hormes, and N.G. Bazan.
5. Poster: "Monitoring potential cytotoxic effects of biomagnetics particles" M.A. DeCoster, J. Cliffe, B. Daniel, and N.G. Bazan.

LSUHSC – DARPA BioMagnetics Project

Project 2: Protection against laser-induced retinal injury. William C. Gordon, PhD

1. Project Area:

Development of a drug delivery system designed to deliver small volumes of highly concentrated pharmacologic compounds to specific tissues utilizing biomagnetic nanopartical technology.

2. Task Objectives:

A) Development of a light-induced retinal damage model.
B) Retinal neuroprotection by an LAU compound.
C) Localization of [^{3}H]leucine-labeled super paramagnetic nanoparticles and directed delivery to specific tissue by a magnetic field.

3. General Methodologies:

Light damage model

To study retinal damage and test neuroprotective compounds, we have constructed a preliminary fluorescent light stimulator consisting of an array of eight circular fluorescent light bulbs, 10 inches in diameter (*figure 1*), which supplies 18,000 lux. Rats were placed within this array for five hours, after which they were returned to darkness until retinas were collected.

Retinal neuroprotection

LAU-0901, a platelet activating factor receptor blocker, is neuroprotective in brain. Following one intraperitoneal injection (30 mg/kg body weight in 45% cyclodextrin in saline) two hours prior to light stimulation, rats were exposed to five hours of light and returned to darkness until retinas were analyzed.

[^{3}H]leucine binding to super paramagnetic nanoparticles

Ten-nm-diameter super paramagnetic nanoparticles were fabricated for us by CAMD and amino groups attached to the surfaces. Under the guidance of CAMD, we attached [^{3}H]leucine to these groups to make it possible to localize the particles within tissues by scintillation counting. Five mg of nanoparticles were dispersed in 0.5 ml distilled water and sonicated under nitrogen for two min. Carbodiimide (4.2 mg; Sigma), dissolved in 0.15 ml water was added and the mixture sonicated for two min. After cooling on ice, [^{3}H]leucine (2.5 to 50 µCi in 125 µl water; SA = 125 Ci/mmol) was added and the sample incubated for two hours at 4^0 C. The nanoparticles were retained on the sides of the reaction tube with a magnetic field and washed with 0.5 ml water five times until minimal radioactivity was detected. Under these conditions, 10% of the [^{3}H]leucine was bound to the nanoparticles.

Directed delivery and localization of nanoparticles in vivo

Labeled nanoparticles were resuspended in 0.5 ml saline, sonicated for five min, and 50 µl injected into the femoral vein of anesthetized adult male mice. These mice were then placed on the surface of a 300 G magnet (Molecular Probes) for one hour with one eye contacting the surface, or one ear taped flat to the magnet. Mice were killed and tissue rapidly collected. The "magnet" ears and eyes were compared to the "nonmagnet" ears and eyes. Also, blood, urine, lungs, kidney, liver, brain, and fat were collected. Tissues were solubleized and aliquots analyzed by scintillation counter for levels of tritium (presence of nanoparticles).

4. Technical Results:

We have shown that when rats are placed in a plastic tube within the light stimulator for 5 hours, photoreceptor death is initiated. Within three days, photoreceptors have undergone apoptosis and have been removed (*figure 2*).

We have shown that pretreatment with the LAU-0901 compound protects photoreceptor cells from light-induced apoptotic death. This compound offers 50-75% photoreceptor neuroprotection (*figure 3*).

We have shown that radio-labeled nanoparticles can be administered systemically and, with the use of a magnetic field, concentrated within specific tissues; the "magnet" ear stuck to magnetic forceps while the "non-magnet" ear did not. Preliminary results from scintillation counts of tissues reveal that within one hour following injection of labeled nanoparticles, approximately half of the label was present in urine. However, some label was retained in liver and lungs. This preliminary study demonstrates that the various organs differentially retain the radio-label, and that the kidneys can actively remove it, suggesting that the problem of tissue toxicity may be minimal. A tissue-specific time course following nanoparticle injection will clearly define these parameters. This is being done now.

5. Importance of Findings and Conclusions:

This first year we have accomplished our "Task Objectives" in that we have a functioning light damage model with which we have demonstrated that we have a photoreceptor neuroprotective compound that can be used in later phases of this study. Moreover, drug-labeled super paramagnetic particles can be directed systemically to localize within specified tissues with a magnetic field. *Proof of principle has been established.*

6. Technical Problems Encountered:

We have attempted to fabricate an electromagnet by wrapping lacquered copper wire around an iron rod and connecting this to a variable power supply. The end of the iron rod was machined so that it would fit onto the cornea of the mouse eye much like a contact lens, allowing the full force of one pole of this bar magnet to impinge on the eye. It was hoped that this would maximally concentrate the nanoparticles within the capillaries of the retina. However, when activated, the iron bar got so hot that it could not be touched. This must be modified. As a partial solution, we are purchasing very strong permanent small diameter bar magnets. These may solve the problem.

7. Implications for Further Research:

Nanoparticles *can* be concentrated within specific tissues with magnetic fields. The obvious implication is that better ways of attaching and releasing compounds of interest must be found or the nanoparticles themselves altered to best deliver the pharmacological compounds. Moreover, more molecules should be attached to each nanoparticle. Now that we have shown that these submicroscopic nanoparticles can be radiolabeled, followed, and quantified, further collaborations with the research units at CAMD and AMRI may accomplish this. In addition, collaborations with an outside group(s) may become necessary to aid in the design of appropriate magnets that are "tissue adapted" for maximum efficiency. Finally, a long term analysis of radio-labeled particles within tissues will inform us of the ultimate destinations of these particles, their tissue half-lives, and whether they remain sequestered within tissues or are eliminated. It will become important to define nanoparticle-related toxicity.

8. Presentations Relating to this Study:

Mardis Gras DARPA meeting; JW Marriott Hotel, New Orleans, LA; 19-20 Feb, 2004:

Bazan NG. *Overview of the biomagnetics project at LSUHSC* - platform

Gordon WC, Bazan NG. *Retinal protection against laser-induced injury* - poster

Association for Research in Vision and Ophthalmology (ARVO); Ft Lauderdale, FL; 25-29 Apr, 2004:

Gordon WC, Cortina MS, Bergsma DR, Ragbir ST, Bazan NG. *Neuroprotection by LAU-0901 in light-induced retinal damage: rod and cone photoreceptor sparing* - poster

Lopez-Osa D, Gordon WC, Cortina MS, Bazan NG. *Ellipsoid mitochondrial fission in light-induced photoreceptor apoptosis* - poster

Cortina MS, Lukiw WJ, Bergsma DR, Gordon WC, Bazan NG. *DNA polymerase (and ß expression selectively localized to photoreceptors is down-regulated by LAU-0901, coinciding with light damage protection* - poster

Mathew B, Gordon WC, Cortina MS, Bergsma DR, Lukiw WJ, Bazan NG. *Efficiency of photoreceptor DNA polymerase (and ß upregulation declines with age* - poster

BioMagnetICs Quarterly Review meeting; Center for Advanced Microstructures and Devices (CAMD), Baton Rouge, LA; 18 Aug, 2004:

Gordon WC, Bazan NG. *Imaging biomagnetic probes in the retina to assess light damage* - poster

Society for Neuroscience; San Diego, CA; 23-27 Oct, 2004:

Cortina MS, Gordon WC, Lopez-Osa DR, Bazan NG. *Mitochondrial DNA repair enzymes up-regulated by oxidative stress in human RPE cells* – poster – to be presented

Lopez-Osa DR, Gordon WC, Cortina MS, Bazan NG. *Mitochondrial fission and apoptosis in light-damaged photoreceptors* – poster – to be presented

Manuscript:

Cortina MS, Gordon WC, Lukiw WJ, Bazan NG. *Oxidative stress-induced retinal damage up-regulates DNA polymerase gamma in photoreceptor synaptic mitochondria*. J Cell Death Different. Submitted. Sept 2004.

9. Tables, Figures, and Descriptions:

Figure 1.

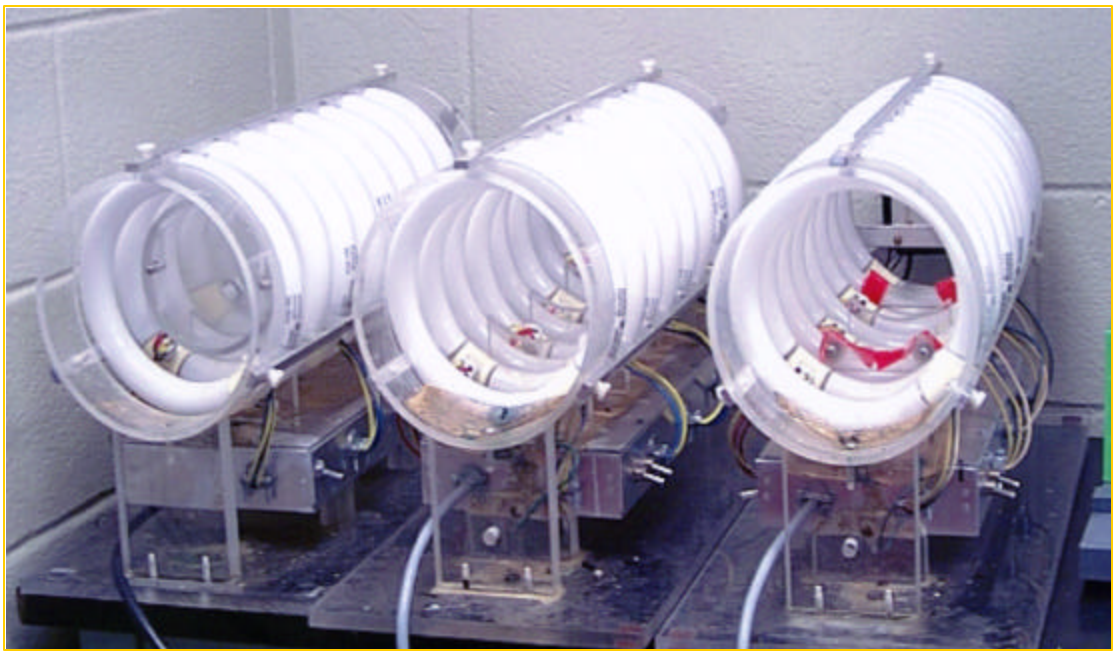

Light stimulators. Each device is composed of an eight bulb array. Animals are placed within a plastic holding tube that is arranged at the center of the device (a plastic tube is visible in the left array). These lights provide 18,000 lux. Five hours of stimulation, followed by a long enough period for photoreceptors to die and drop out, induces about 50% loss.

Figure 2.

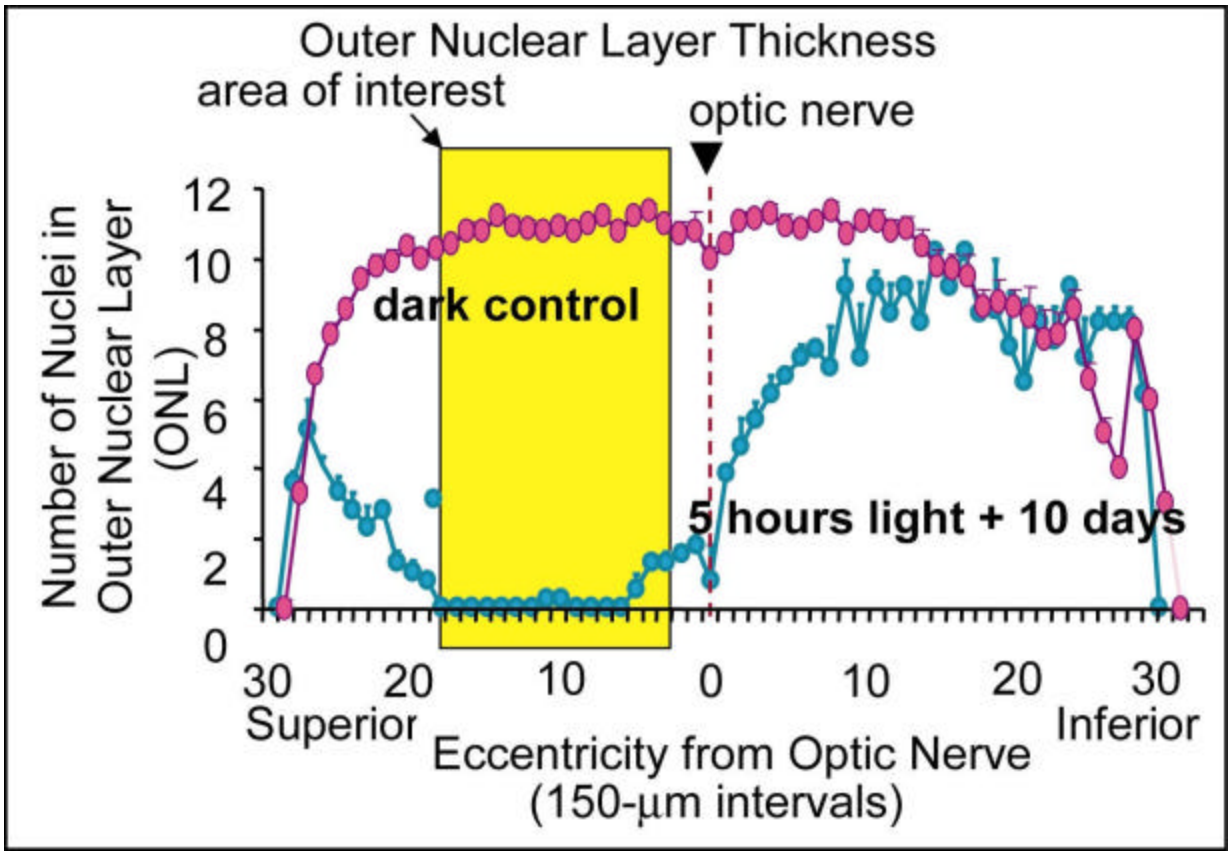

Photoreceptor loss following light damage treatment of rat retina. The number of photoreceptor nuclei across the retina from the superior edge to the inferior margin are plotted. Normal, healthy retinas have outer nuclear layers (ONL) that are 12 nuclei thick (*red curve*). At 10 days following 5 hours of light damage treatment the superior central portion of the retina (the "sensitive" region) exhibits massive cell death and loss (*blue curve; yellow region*).

Figure 3.

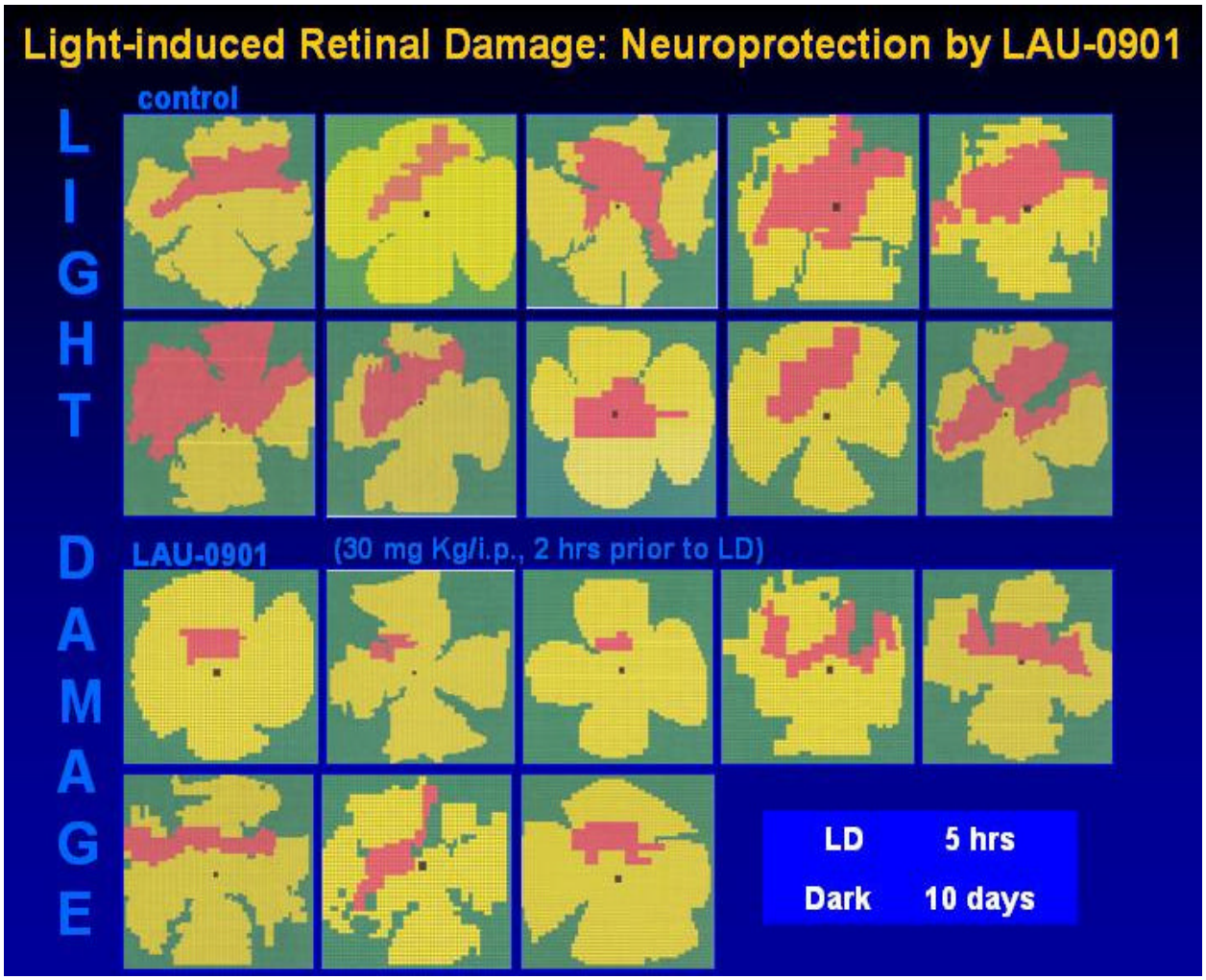

Light-induced retinal damage fields in rat retina. Following 5 hours of light treatment plus 10 days, retinas were collected and flattened with 4 radial cuts. A molecular marker was used to label photoreceptors. Each retina was scanned in x and y coordinates and each microscope field was scored for presence or absence of photoreceptors. Normal retina is denoted in *yellow*, photoreceptor loss is shown in *red*. Black indicates the position of the optic nerve. The upper 10 retinas show normal light damage following 5 hours of light treatment. The lower 8 retinas were pretreated with LAU-0901 prior to light treatment. Notice the reduction in area of cell loss with pretreatment. LAU-0901 offers 50-75% protection from light-induced photoreceptor loss.

LSUHSC – DARPA BioMagnetics Project

Project 3. Pain in the Military Personnel

1. **Task Objectives**:

The following objectives will be done at LSUHSC-NSC

- ✓ To develop candidate analgesic compounds that bear a carboxyl group to be linked to magnetic nanoparticles
- ✓ To test the new compounds for analgesia
- ✓ To test for liver toxicity.
- ✓ To bind the analgesic to nanoparticles at CAMDI
- ✓ To test *in vitro* the inhibitory effect of the analgesic alone and linked to nanoparticles in the COX-2 enzyme
- ✓ To test *in vivo* analgesic effect of the analgesic alone and linked to nanoparticles in a model of pain

2. **Technical problems encountered**.

To date, one compound (SCP-22) derived from SCP-1 has been prepared and tested for analgesic activity, liver toxicity and its inhibitory action on COX-2 enzyme. Because low amounts are generated through chemical synthesis and subsequent binding to NP, no studies given the drug ip or iv can be performed. Therefore, to allow us to study the effects of the drug in small quantities in vivo the NP bound compounds were administered intrathecally (ie., spinal).

3. **General Methodology**

a. ***Pain assays***. *Chemically-induced writhing.* In this model of visceral pain, abdominal contractions (writhing) were induced in mice by an IP injection of 0.4% acetic acid at a dose of 10 ml/Kg. The numbers of writhes, characterized by a wave of contraction of the abdominal muscles followed by extension of the hind limbs, were counted for 10 min beginning 5 min after the acetic acid injection. *Complete Freund's Adjuvant-Induced Thermal Hyperalgesia.* Under halothane anesthesia, mice were injected with 0.1 ml of CFA (Calbiochem, USA) to the glabrous surface of one hind paw. When injected into the

foot-pad, CFA produces localized inflammation and hyperalgesia that appears within 2 h and is present for 7 to 10 days. At 48-hours post-CFA (time of peak hyperalgesia) the latency to withdraw the paw from a thermal stimulus was measured using an analgesiometer (IITC Life Sciences, Inc, Woodland Hills, CA). The stimulus intensity will be set to produce baseline latencies of about 10-15 sec, and a 20 sec maximum latency will be used. Thermal hyperalgesia was measured before (pre-drug baseline) and after drug administration.

b. Toxicity assays. *Serum transaminase activity (GPT/GOT).* After sacrifice, blood was withdrawn into heparinized 1 cc capillary syringes. The blood samples will be spun at 3000 rpm for 10 min in a refrigerated centrifuge to separate plasma. The GPT and GOT levels were determined spectrophotometrically using Sigma kits. *Glutathione depletion.* After sacrifice, the livers will be perfused with heparinized saline. The right half of the main lobe was removed and homogenized using Teflon pestle in MPA (5% w/v) to a concentration of 5% (w/v). The homogenate was centrifuged at 3000 G for 10 min at 4^oC, and glutathione levels were measured in duplicate on 300: 1 aliquots of the supernatant using a standard colorimetric assay.

c. COX-2 assay in HUVEC's cells. HUVECs were obtained from BioWhittaker (Cambrex). Cells were used in passage 3-7. Cells were grown in EGM2 (BioWhittaker, Cambrex) to75-85% confluence in a 37^0C incubator/CO_2 5% and then plated in 6-wells plates. For COX-2 induction, the cells were starved overnight in EBM + 2% FBS followed by 24 h incubation in EGM2 media containing 2% FBS prior to the addition of IL1 alpha (4 µl, 2µl/ml in 0.9% saline containing 1%BSA). The media from HUVECs cultures activated with IL1 alpha was changed to Hank's solution, 0.75% BSA. SCP-22 suspended in DMSO/media and SCP-22 bound to NP suspended in media was added to the wells (20 µl; final conc. DMSO in the wells 0.01%). Controls received the same volume of the vehicle (DMSO or NP). After 30 min incubation at 37^0C in a shaking incubator, AA was added (final conc 2 µM) and the cells further incubated for 15 min. The media was collected for prostaglandin E_2 (PGE_2 analysis by EIA (Cayman) following the kit instructions.

4. Technical Results

Analgesia: Of the 3 synthesized compounds that beared the requisite carboxyl group, one compound SCP-22 (Figure 1) showed good analgesic activity. A 3 mmol/kg oral dose of SCP-22 showed analgesic activity that was confirmed in 2 pain assays (Complete Freund's Adjuvant-induced hyperalgesia and chemically-induced writhing, Figures 2 and 3). Because low amounts of SCP-22 are generated through chemical synthesis (see Technical Problems above) the analgesic effects were also determined for SCP-22 when administered intrathecally (at 15 minutes post injection). It was found that when administered intrathecally SCP-22 retained it's analgesic effect (Figure 4).

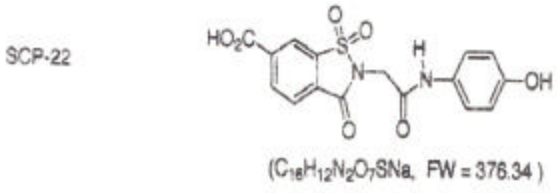

Figure 1. Structure of SCP-22

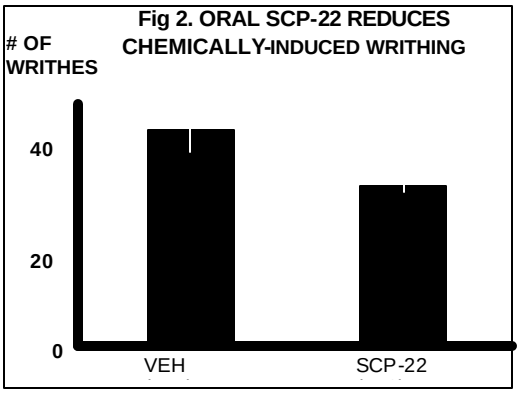

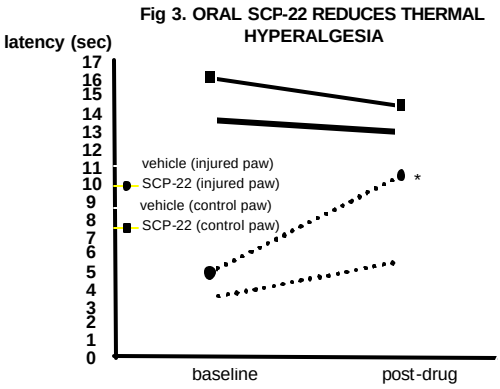

Figure 4. Analgesic Effects of Intratecal SCP-22

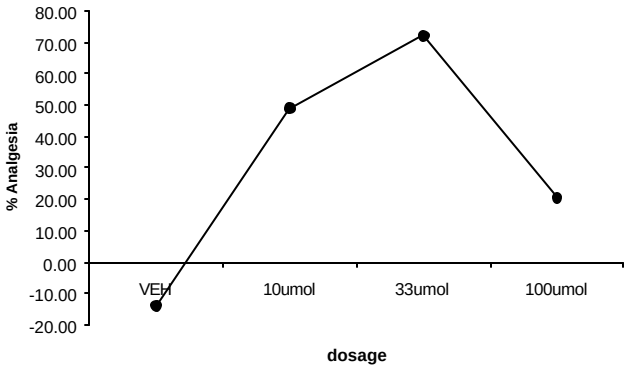

***Toxicity*:** A 6 mmol/kg oral dose of compound #22 did not produce hepatotoxic effects (it did not deplete liver glutathione and did not elevate plasma transaminase activity, Figure 4 and Figure 5).

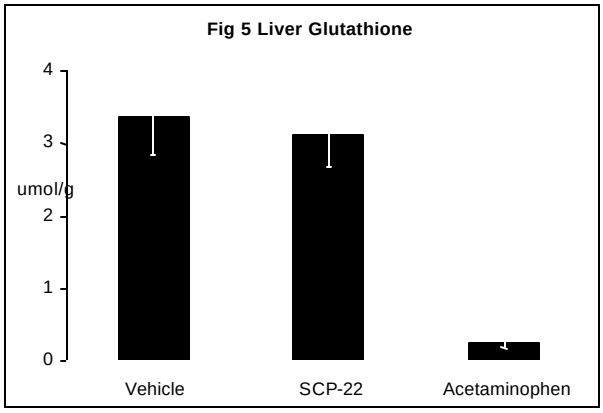

Fig 6. Plasma Transaminases

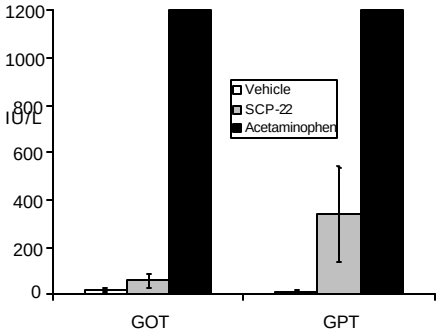

Binding of Analgesic to Magnetic Nanoparticles: Because SCP-22 has a carboxyl group in C2 (see Figure 1) and showed good analgesic activity and low toxicity, the possibility

of binding this drug to magnetic nanoparticles was explored. SCP-22 was sent to CAMD and Dr. Challa Cumar linked the drug to magnetic nanoparticles (MNP) using carbodiimide chemistry. The drug-NP complex sent from CAMD to LSUHSC contained 3.7 mg of SCP-22 bound to 24 mg drug-NP. Analysis by HPLC at CAMD indicated that the drug was successfully bound to MNP.

***In vitro activity of SCP-22-MNP (Inhibition of COX-2 enzyme)*:** The biological activity of the bound drug as inhibitor of COX-2 was tested in HUVEC's cells. SCP-22-NP did inhibit COX-2 although with less efficiency than SCP-22 in DMSO (**Table 1**). Although a shaker incubator was used, there was not a good homogeneous distribution of the drug-NP above the cells. This could explain the lower inhibitory effect as compared to drug/DMSO.

	Control	SCP-22, 200 µM
	Mean ± SD	Mean ± SD
A	n=6	n=6
In DMSO	266 ± 34	166 ± 15
In NP	211 ± 48	155 ± 12
B	n=12	n=12
In DMSO	100	56.8 ± 7.1
In NP	100	73.1 ± 5.1

Table 1. SCP-22 inhibition of COX-2 bound to magnetic nanoparticles as compared to SCP-22 dissolved in DMSO. A, pg PGE_2/ml; B, percent to control values. Mean values ± SD are shown from the number n of individual determinations

***In vivo activity of SCP-22-MNP (Analgesia)*:** The biological activity of SCP-1 bound to nanoparticles was determined after intrathecal administration in the CFA assay. It was found that SCP-22 retained it's analgesic effects when bound to MNP (Fig 7)

Fig 7. Analgesic effect of SCP-22+MNP

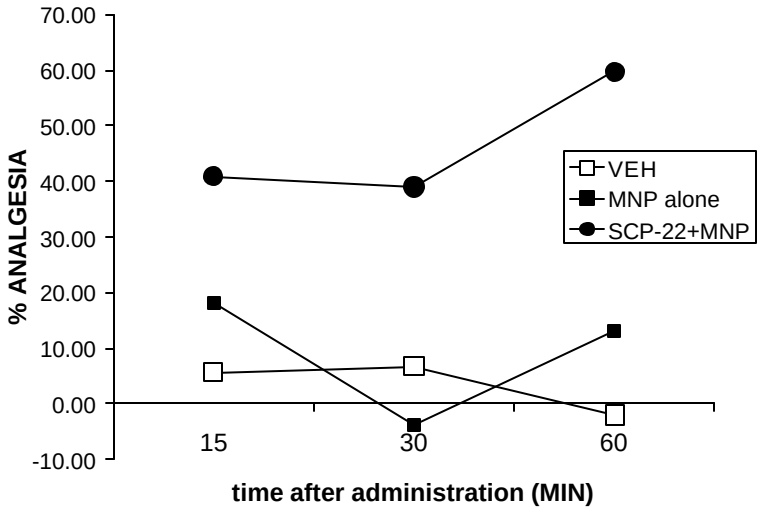

5. Importance of findings and Conclusions:

The results obtained with the drug bound to nanoparticles indicates that the drug retains its biological activity both *in vitro* and *in vivo*, and suggests that SCP-22 is a good candidate to further explore this new approach of drug delivery in pain assays.

6. Implications for further Research.

Future research will be designed to determine whether technology can be used to target pain and inflammation with great specificity without harmful side effects.

7. Publications and Presentations

Vaccarino, A.L, D. Paul, P. Mukherjee, E.B Rodríguez de Turco, V.M. Marcheselli, L. Xu, M.L. Trudell, J. M. Minuéz, C. Sunkel, J. Alvarez-Builla & N. G. Bazan, Synthesis of non-hepatotoxic acetaminophen analogs with high analgesic and anti-pyretic properties, Journal of Medicinal Chemistry, under review.

Vaccarino, A.L., E.B. Rodriguez de Turco, F. Jackson, N. Parking, M.L. Trudell, HA. Scuderi, M.S. Calhoun & N. G. Bazan, Development of Analgesic-Magnetic Nanoparticles for drug delivery, BioMagnetics PI Review , MD, 2004.

Vaccarino, A.L. & N.G. Bazan, Development of novel analgesics with minimal side-effects, NSF-EPSCOR Capitol Day, Baton Rouge, LA 2004.

Vaccarino, A.L. H.A. Scuderi, M.S. Calhoun & N.G. Bazan, Use of biomagnetics in the treatment of pain in military personnel, Defense Advanced Research Agency Biomagentics Meeting, New Orleans, LA, 2004.

Vaccarino, A.L., M.L. Trudell, E.B. Rodriguez de Turco, H.A. Scuderi, J. Alvarez-Builla, C. Sunkel & N. G. Bazan, Development of novel non-steroidal analgesics for post-surgical pain, Society for Neuroscience Abstracts, 2003.

PART 4 – Xavier University Report

Bio-Magnetics Interfacing Concepts: A Microfluidic System using Magnetic Nanoparticles for Quantitative Detection of Biological Species

(Subcontractor: Xavier University of Louisiana)
Xavier University of Louisiana
1 Drexel Drive
New Orleans, LA 70125-1098

Subcontract to Xavier University – Nitsa Rosenzweig
(until 04/2004) and AMRI-UNO (05/2004-08/2004)

The work at Xavier University of Louisiana included collaboration with Professor Zeev Rosenzweig from AMRI at the University of New Orleans Chemistry Department. The collaborative effort concentrated on developing new nanocomposite particles that consist of polymer coated-Fe2O3 superparamagnetic cores and CdSe/ZnS quantum dots (QDs) shell. Our objective was to demonstrate the utility of these particles in separating breast cancer cells from aqueous buffers and physiological fluids. To accomplish this goal we immobilized anti cycline E antibodies on the particles surface and use the antibody coated particles to separate MCF-7 breast cancer cells from serum solutions. Anti cycline E antibodies bind specifically to cycline, a protein which is specifically expressed on the surface of breast cancer cells. The separated breast cells were easily observed by fluorescence imaging microscopy due to the strong luminescence of the luminescent/magnetic nanocomposite particles. This work was published recently in the journal nanoletters (CdSe/ZnS Quantum Dots-Magnetic Beads Core-Shell Nanocomposite Particles for Cell Separation" *Desheng Wang1, Jibao He2, Nista Rosenzweig3 and Zeev Rosenzweig1)* and is described in detail in the section "AMRI – Main Project 2).

Since moving to AMRI-UNO in May 2004 I established a tissue culture lab with all the necessary equipment to grow cell lines as well as primary cells and tissue. I also established a Biomagnetics research group that consist of postdoctoral fellow Silvia LaCerda and Abdul Hamide, a lab technician. Our objective is to develop magnetic nanoparticles that are coated with biodegradable biopolymers for drug targeting and controlled drug release. Initial studies used gold nanoparticles since protocols to coat gold nanoparticles with proteins are well established. Figure 1 shows TEM and SEM images of collagen coated particles. While certain degree of aggregation is seen the particles appear spherical in shape and show rather smooth morphology

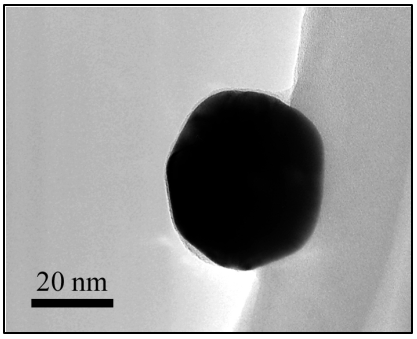

Figure 1a - A TEM Image of a single collagen-coated gold nanoparticle

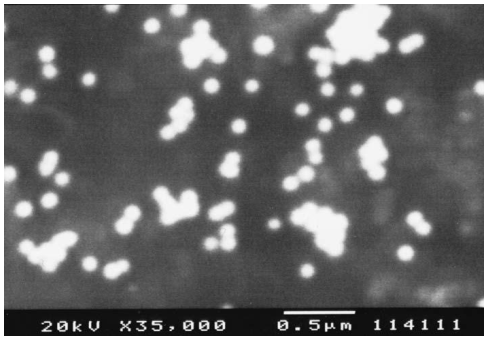

Figure 1b – An SEM image of collagen coated gold nanoparticles

The next phase of the study will focus on conjugation the biopolymers to magnetite and gold coated iron particles. Furthermore, the particles will be loaded with drug molecules,

conjugated to targeting biomolecules (e.g antibodies) and used as drug delivery vehicles. An important step to accomplish this long term goal is to establish that collagen coatings could be loaded with physiologically relevant amounts of drugs and their release properties could be controlled. Initial studies in this area focused on the preparation of collagen gels that were loaded with the fluorophore rhodamine 6G, which served as a drug analog. Release properties of the gels were attenuated by modifying the type and amount of cross linking molecules used to stabilize the collagen gels. Figure 2 shows the results of uptake of rhodamine 6G into collagen gels containing increasing concentrations of the cross linker chondroitin-6-sulfate.

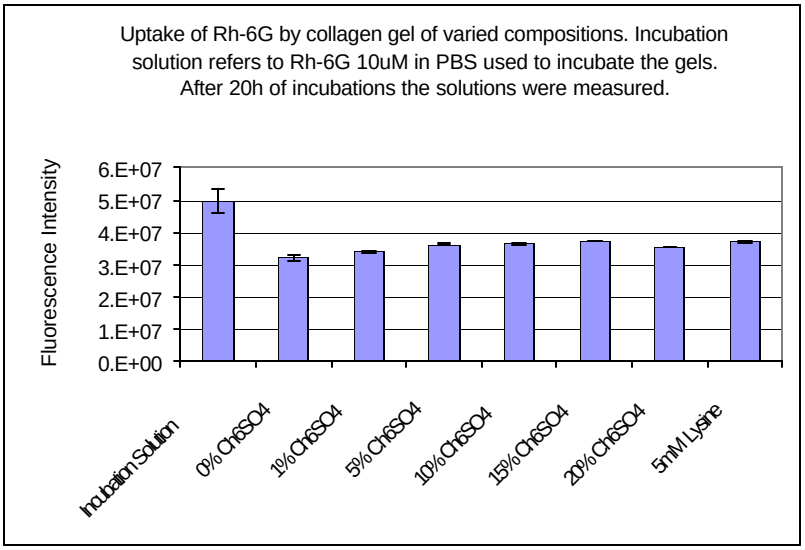

Figure 2 - uptake of rhodamine 6G into collagen gels containing increasing concentrations of the cross linker chondroitin-6-sulfate.

It can clearly be seen that the gels were loaded effectively with rhodamine 6G regardless of the level of chodroitin-6-sulfate. This is an important finding that suggests that attenuating the level of chodroitin-6-sulfate could be used to control the release properties of the gels in wide range of desirable release kinetic profiles without significantly affecting the drug level in the gel.

Figure 3 describes the results of release studies of rhodamine 6G from the collagen gels that contain increasing levels of chondroitin-6-sulfate.

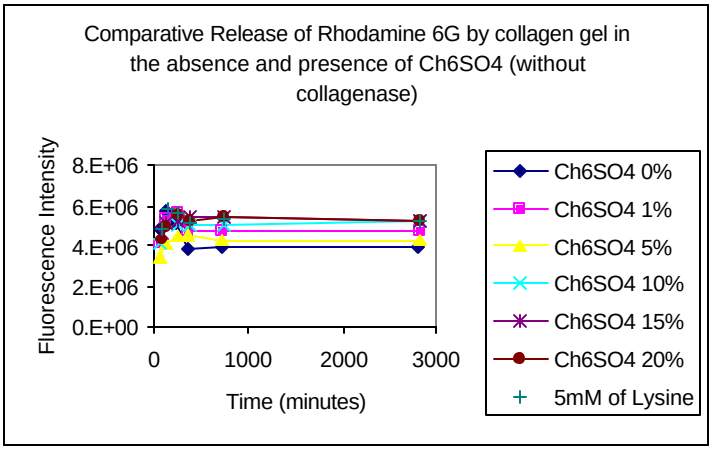

Figure 3 – Release measurements of rhodamine 6G from collagen gels containing increasing levels of chondroitin-6-sulfate.

It can be seen that the release rate is larger as the concentration ofchondroitin-6-sulfate increases. This is attributed to an increase in pore size of the gels with increasing levels of cross linker. Future studies will focus on quantization the effect of different cross-linkers to better control the time-release properties of anti cancer drug. We will also synthesize drug-containing collagen particles and study their release properties. Finally, magnetic nanoparticles will be incorporated into the collagen particles to facilitate targeting and localization of the drug containing particles in tissue cultures and in in-vivo studies using externally controlled magnetic fields.

Publications

"CdSe/ZnS Quantum Dots-Magnetic Beads Core-Shell Nanocomposite Particles for Cell Separation", Desheng Wang, Jibao He, Nitsa Rosenzweig and Zeev Rosenzweig, Nano Letters (2004) 4(3); 409-413.

Presentations

"Luminescent/Magnetic nanoparticles in Bioassays", Desheng Wang, Nitsa Rosenzweig and Zeev Rosenzweig, Pittcon 2004, New Orleans, LA, March 2004.

PART 5 – MagneSensors Report

Bio-Magnetics Interfacing Concepts: A Microfluidic System using Magnetic Nanoparticles for Quantitative Detection of Biological Species

(Subcontractor: MagneSensors, Inc.)
MagneSensors, Inc.
9717-A Pacific Heights Blvd
San Diego, CA 92121

FINAL REPORT

Prepared for
Lousiana State University and Agricultural and Mechanical College
Acting for the University of New Orleans

Subaward number: 02-238-S4
Defense Advanced Research Projects Agency (DARPA)
Bio Magnetics Interfacing Concepts

Period of performance:
August 26, 2003 - August 26, 2004

MagneSensors Contract Number 3021

Mark S. DiIorio, Ph.D.
(858) 458-5750
markd@magnes.com

MagneSensors, Inc.
9717-A Pacific Heights Blvd.
San Diego, CA 92121

September 22, 2004

Task Objectives

MagneSensors' SQUID-based magnetic detection platform was used to evaluate magnetic nanoparticles prepared by AMRI.

The specific tasks included:

1) Measure the magnetic signal from different magnetic nanoparticle preparations
2) Titrate magnetic nanoparticle concentration to determine the minimum detection limit,
3) Measure multiple magnetic nanoparticles samples with same concentration to evaluate (indirectly) variation in magnetic nanoparticle preparation
4) Examine impact of sample preparation on magnetic signal

The magnetic measurement was used to determine key nanoparticle parameters including:

- magnetic relaxation signal
- detection limit (minimum number of nanoparticles)
- reproducibility of nanoparticle preparation
- agglomeration
- best methods for handling nanoparticles (vortexing, sonication)

Methodology

MagneSensors' used a custom designed high temperature SQUID based instrument (see Fig. 1 and Fig. 2) that measures the magnetic signal as a function of time for magnetic nanoparticles located in microtiter wells. The instrument is computer controlled with custom software for the acquisition and signal processing the magnetic data.

The high sensitivity enables us to measure magnetic nanoparticles located a short distance from the sensor (0.5 - 2 mm). Each sample measurement takes a few seconds, which can be readily extended to take data over a longer time period.

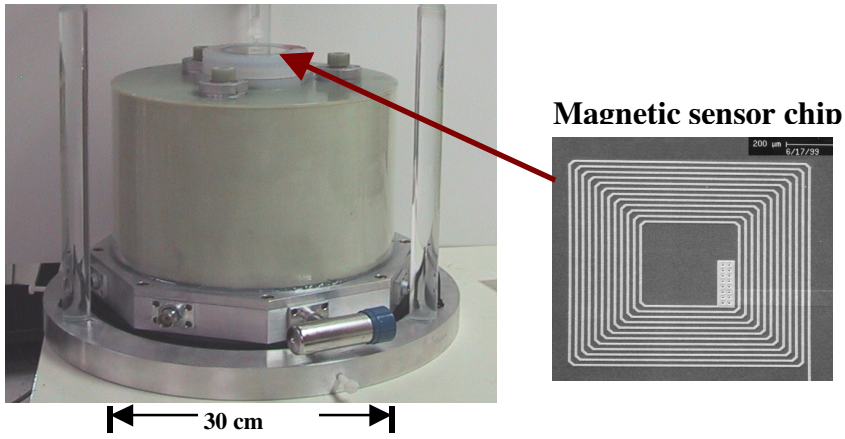

Fig. 1 System photo of SQUID based detection instrument for magnetic assays. Size scale is shown at the bottom. Portion of sensor chip is shown on the right.

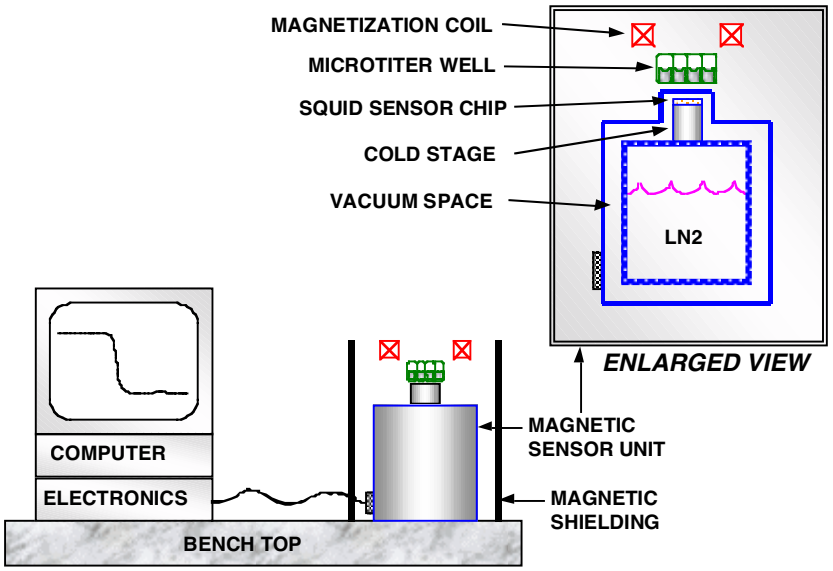

Fig. 2 System diagram of SQUID based magnetic detection test bed. The entire instrument is located in a magnetic shield to prevent unwanted external noise sources from interfering with the sensitive measurements.

For these measurements, individual wells are used.

The measurement procedure is outlined in Fig. 3. A microplate well, which contains the sample to be measured, is mounted on the end of a non-magnetic sample stage. The stage is mounted inside the magnetic shield containing the SQUID instrument and the magnetization coil.

The sample is moved into the magnetization coils and a demagnetization field (not shown) is first applied for a few seconds in order to zero the moment of the sample. The magnetization field is applied, typically 20-60 G, for 1-2 seconds.

After the magnetization coil is turned off, the SQUID instrument begins acquiring data as the sample is moved toward the sensor. We thus measure the magnetic moment of the magnetic nanoparticles (the SQUID measures a *change* in field) and by acquiring data over time a relaxation curve is obtained. The remnant field is measured by moving the sample away from the instrument.

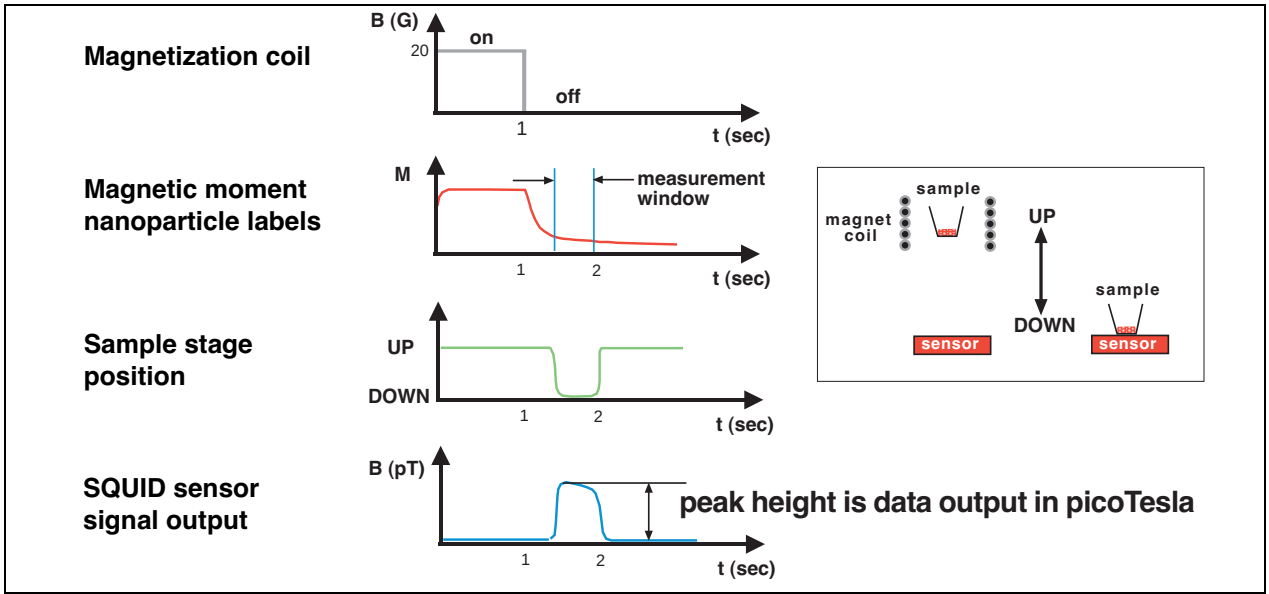

Fig. 3 Measurement procedure for acquiring magnetic data using SQUID instrument.

The magnetic nanoparticles need to be "bound" to a solid support in order to give a signal in our time window of measurement. The magnetite samples were prepared by suspending particles in Phosphate Buffered Saline (PBS) for dilution and drying various concentrations of diluted particle solutions in standard microwells for magnetic characterization. We used methanol instead of PBS for preparing the permalloy samples.

Technical Results

The magnetic nanoparticles provided by AMRI that were measured included:

- Silica coated magnetite 12 nm diameter nanoparticles
- Gold coated permalloy particles ($Fe_{20}Ni_{80}$) 8 - 10 nm diameter nanoparticles

The key results are summarized below:

1) The magnetic signal (per nanoparticle) from the best samples of the two types of magnetic nanoparticles provided is comparable. The detection limit is near 10^9 nanoparticles.
2) The magnetic signal for these small nanoparticles was not yet large enough to use as labels in magnetic assays; it is two orders of magnitude weaker than the 140 nm magnetic nanoparticles we currently use (after scaling for the differences the amount of magnetite in each nanoparticle).
3) There is a remnant signal from the nanoparticles indicating that a number of them are in close proximity (inter-particle coupling); otherwise the 8-12 nm nanoparticles are superparamagnetic and the signal would decay to zero by the time we measure it.
4) For permalloy particles, vortexing in addition to sonication helps to suspend particles more uniformly resulting in less agglomeration and more reproducible results
5) Different preparations of the permalloy nanoparticles give different magnetic signals; one batch had 100X better signal than the other. This should help with optimizing the preparation of the nanoparticles.

Data is shown in Fig. 4 and Fig. 5 for the silica coated magnetite nanoparticles. Fig. 4 shows a typical magnetic relaxation signal for the magnetic nanoparticles. The fact that any remnant signal exists must be due to inter-particle coupling, or a smaller number of larger conglomerate particles, since a 12 nm diameter nanoparticle is below the superparamagnetic limit and thus should have no remnant signal. The reproducibility of the data on different samples makes it less likely that there are large agglomerates, but the large number of nanoparticles in each sample means we cannot rule it out. We did not visually notice agglomeration upon sample preparation.

Fig. 5 shows the magnetic signal as a function of the number of magnetic nanoparticles in the well. Four different samples are measured for each data point and the coefficient of variation (%CV) for these samples (10-20%) is fairly good showing reasonable reproducibility for magnetite. The detection limit (about 500 fT for our system in the configuration used) is about 1 x 10^9 nanoparticles, which after scaling for the mass of the magnetic nanoparticle is about two orders worse than 140 nm (hydrodynamic diameter) Fe_3O_4 magnetic nanoparticles we obtain commercially from Molecular Probes. However, the AMRI nanoparticles were measured in a 60 G magnetic field, which is 2-3X higher than our typical applied magnetization field and increases the signal by the same factor.

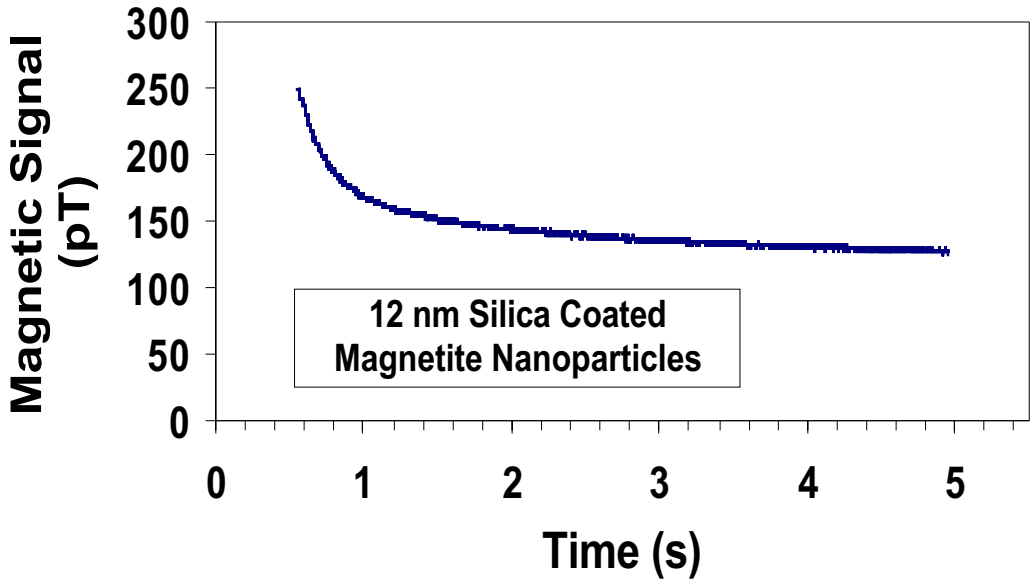

Fig. 4 Magnetic relaxation signal as a function of time for 12 nm silica coated magnetite nanoparticles.

There are a number of assumptions that we have to make in order to obtain the number of magnetic nanoparticles per unit volume. These have some uncertainty, but are unlikely to have a major impact on the results that we obtain. AMRI reports that the nanoparticle core diameter is 12 nm and the material supplied is 0.2 mg/ml Fe_3O_4. The former is used to calculate the theoretical mass of Fe_3O_4 per particle. The ratio of the mass/nanoparticle to the mg/ml supplied yields the number of nanoparticles per supplied liquid volume, which here is 4.3 x 10^{10} nanoparticles/µl.

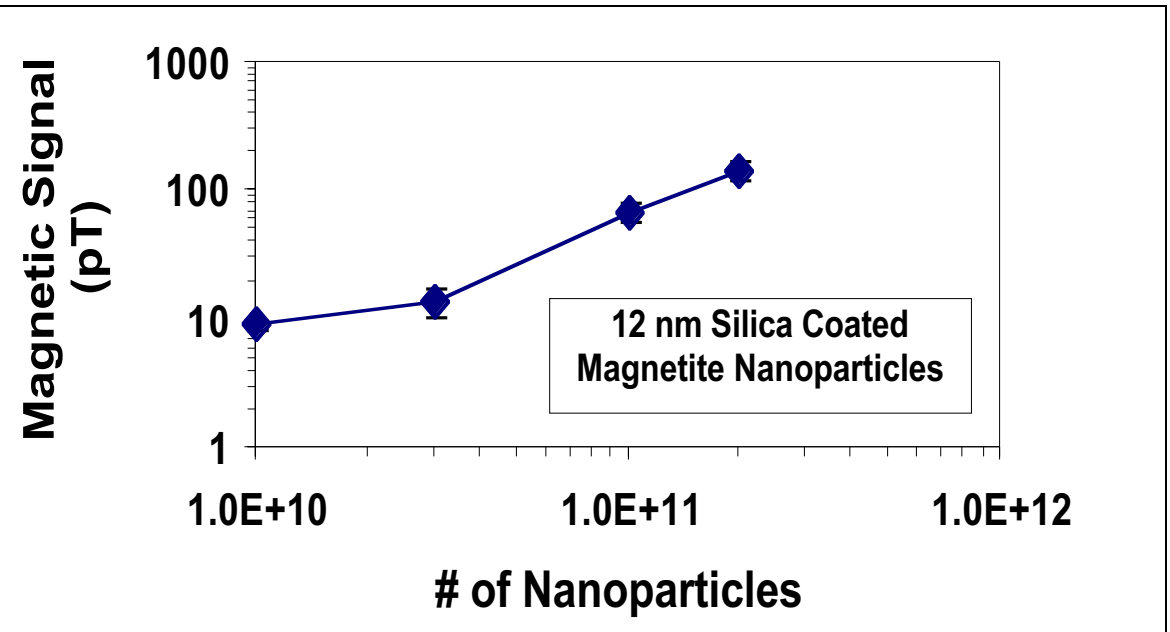

Fig. 5 Magnetic signal (single point remnant field measurement) as a function of nanoparticle number for 12 nm silica coated magnetite nanoparticles. Samples prepared in quadruplicate.

The permalloy nanoparticle samples that we measured were supplied in three shipments:

Batch #1 November 14, 2003

Batch #2 July 4, 2004

Batch #3 July 14, 2004.

Measurement results are shown in Table 1. Each data point is the average of 40 samples. The remnant signal from batch #2 was two orders of magnitude higher than the other two batches. Consequently, AMRI can examine the preparation to learn what was done in the processing to make this batch different from the others.

When scaled to magnetic field per nanoparticle, the batch #2 signal is 110 pT / $1x10^{11}$ particles, which matched roughly with signals from 12 nm magnetite samples (69 pT / $1x10^{11}$ particles). Demagnetization was performed on all samples prior to magnetization and measurement. The demagnetization and magnetization fields were both 60 G.

The sample preparation is of interest since we found that different combinations of agitation improved the reproducibility of the data, presumable due more uniform suspension of the nanoparticles. Sample reproducibility is clearly a concern as shown by the %CV numbers below.

Roughly 10 mg of powders from each shipment were weighted and a volume of methanol was added to give 5 $x10^{12}$ particles per 5 ul to be dried in each well. The dry nanoparticle powders were stored in an argon desiccator when not in use.

Three combinations of agitation before pipetting were tested for better sample preparation and well-to-well consistency:

A) **Sonication only** After initial mixing of sample powder: sonication for 1 min; after dispensing into group of 8 wells sonication 10 sec

B) **Short sonication and vortexing** After initial mixing of sample powder: sonication for 10 sec and vortexing 10 sec; nothing further after dispensing

C) **Long sonication and vortexing** After initial mixing of sample powder: sonication 1 min and vortexing 1 min; after dispensing into group of 8 wells: sonication 10 sec and vortexing 10 sec

Agitation used in preparation for measurement		Batch #1	Batch #2	Batch #3
A – Short sonication only	Average Stdev CV (%)		**3900** 5780 148%	
B – Short sonication and short vortexing:	Average Stdev CV (%)	13 4.5 34 %		40 53 130%
C – Long sonication and long vortexing	Average Stdev CV (%)		**5620** 1710 **30**%	34 14 **42**%

Table 1. Magnetic measurement of permalloy nanoparticle samples. Prepared for measurement using different agitation techniques. The data shown is the average of 40 samples of 5 ul aliquots with nominally 5 x 10^{12} nanoparticles per sample.

Increased agitation and mixing significantly reduces the well-to-well variation.. For example, vortexing the sample solution, in addition to sonication, improved batch #2 CVs from 148% to 30%.

The nanoparticle number density was calculated using supplied information and material density as follows. The supplied core diameter (8 - 10 nm) and shell diameter (15 nm) of the particle, together with the permalloy density 8.6 g/cm^3 and Au density 19.3 g/cm^3, were used to calculate the theoretical mass per gold coated permalloy particle. The calculated mass per particle is 2.8 x 10^{-17} g and particle density number is 3.5 x 10^{13} particles per mg of powder.

Technical Problems En countered and Suggested Improvements

The signal from the nanoparticles is fairly low, in large part due to their small size. Increasing the size would help improve the detection limit.

It would also help to measure nanoparticles with functional coatings. With even simple coatings, we can bind the nanoparticles more uniformly on the bottom of the microplates well, which should improve the reproducibility further (drying can produce non-uniform patterns, producing some variation from sample to sample). We can also perform a simple magnetic assay, which is a more stringent test of the suitability of the magnetic nanoparticle for detection.

For all nanoparticles, including those we obtain commercially, there are concerns related to agglomeration. Improved nanoparticles, biological conjugations to the nanoparticle, sample preparation techniques, and buffer solutions should be studied. While serious agglomeration can be seen visually as the nanoparticles settle out of solution, smaller problems can frequently be ascertained from sample variability, and the magnetic measurement is a valuable tool here.

In the end, we expect the magnetite to be superior to the permalloy as there should be fewer problems with agglomeration. The data taken to date reflects this.

Finally, it will be helpful to obtain more nanoparticle samples, allowing better statistics to be obtained.

Publications and Presentations

There have been no publications or presentations yet on this work although it has been discussed in DARPA and AMRI forums.

REPORT DOCUMENTATION PAGE

Form Approved
OMB No. 0704-0188

PLEASE DO NOT RETURN YOUR FORM TO THE ABOVE ADDRESS.

1. REPORT DATE *(DD-MM-YYYY)*	2. REPORT TYPE	3. DATES COVERED *(From - To)*
09/30/2004	FINAL	26 Aug 2003 - 31 Aug 2004

4. TITLE AND SUBTITLE
Bio-Magnetic Interfacing Concepts: A Microfluidic System using Magnetic Nanoparticles for Quantitative Detection of Biolgogical Species

5a. CONTRACT NUMBER
MDA972-03-C-0100

5b. GRANT NUMBER

5c. PROGRAM ELEMENT NUMBER

6. AUTHOR(S)
O'Connor, Charles J., Hormes, Josef, and Bazan, Nicolas G.

5d. PROJECT NUMBER

5e. TASK NUMBER

5f. WORK UNIT NUMBER

7. PERFORMING ORGANIZATION NAME(S) AND ADDRESS(ES)
University of New Orleans
Advanced Materials Research Institute,
2000 Lakeshore Drive
New Orleans, LA 70148

8. PERFORMING ORGANIZATION REPORT NUMBER

9. SPONSORING/MONITORING AGENCY NAME(S) AND ADDRESS(ES)
DARPA/CMO
Attn: James B. Troutman
3701 Fairfax Drive
Arlington, VA 22203-1714

10. SPONSOR/MONITOR'S ACRONYM(S)

11. SPONSOR/MONITOR'S REPORT NUMBER(S)

12. DISTRIBUTION/AVAILABILITY STATEMENT
Approved for public release; distribution unlimited.

13. SUPPLEMENTARY NOTES
The views and conclusions contained in this document are those of the authors and should not be interpreted as representing the official policies, either expressly or implied, of the Defense Advanced Research Projects Agency or the U.S. Government.

14. ABSTRACT
This report describes a research project in the area of bio-magnetics interfacing concepts aimed at developing a microfluidic system based on the use of magnetic nanoparticles for the quantitative detection of biological species in various media. Novel bio-compatible ferrofluids of functionalized magnetic nanoparticles suitable for bioconjugation of antibodies or other active biomolecules are developed, prepared, and tested for use in biomedical research, and various biological and clinical diagnostic applications.

15. SUBJECT TERMS
biomagnetic interfacing concepts, functionalized magnetic nanoparticles, detection of biological species, biocompatible ferrofluids

16. SECURITY CLASSIFICATION OF:			17. LIMITATION OF ABSTRACT	18. NUMBER OF PAGES	19a. NAME OF RESPONSIBLE PERSON
a. REPORT	b. ABSTRACT	c. THIS PAGE			Charles J. O'Connor
U	U	U	UU	77	19b. TELEPHONE NUMBER *(Include area code)* (504) 280-6840

Reset

Standard Form 298 (Rev. 8/98)
Prescribed by ANSI Std. Z39.18